STATISTICAL PHYSICS OF DISLOCATION NUCLEATION BY NANOINDENTATION

by

JEREMY K. MASON

Submitted to the Department of Physics in partial fulfillment of the Requirements for
the Degree of

BACHELOR OF SCIENCE

at the

MASSACHUSETTS INSTITUTE OF TECHNOLOGY

June, 2005
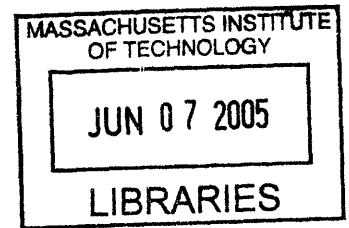
Signature of Author _____

Department of Physics
May 7, 2005

Certified by _____

Assistant Professor Christopher Schuh
Thesis Supervisor, Department of Materials Science and Engineering

Accepted by_____

Professor David E. Pritchard
Senior Thesis Coordinator, Department of Physics

STATISTICAL PHYSICS OF DISLOCATION NUCLEATION BY NANOINDENTATION

by

JEREMY MASON

Submitted to the Department of Physics on May 7, 2005 in Partial Fulfillment of the Requirements for the Degree of Bachelor of Science in Physics

ABSTRACT

Current understanding of the onset of plasticity during nanoindentation of crystalline materials involves homogenous dislocation nucleation in the crystal underneath the indenter. Through the use of cutting-edge nanoindentation techniques, this study examines the initiation of plastic deformation in single crystal oriented platinum samples. Variations in the temperature and loading rate during indentation reveal temporal and thermal dependencies, and support the stochastic and thermally-activated nature of the initial plastic event. These dependencies of dislocation nucleation are precisely quantified by developing analysis methods based on statistical thermodynamics, and are used to evaluate the probability of various atomistic mechanisms. The results of this procedure implicate a critical activation event occurring in a single atomic volume, with an activation enthalpy of a fraction of an electron volt. These findings strongly indicate that the initiation of plasticity begins with a heterogeneous dislocation nucleation event, in conflict with the current belief, and significantly advance understanding of the onset of plastic deformation during nanoindentation.

Thesis Supervisor: Christopher Schuh
Title: Assistant Professor of Materials Science and Engineering

ACKNOWLEDGMENTS

CONTENTS

LIST OF FIGURES

LIST OF TABLES

CHAPTER 1

INTRODUCTION

1.1   MOTIVATIONS FOR INQUIRY INTO DISLOCATION NUCLEATION

Progress in the field of applied physics is marked by the understanding and engineering of physical systems on ever finer scales. The use of surface films to alter the friction or wear characteristics of moving parts, the development of micro-electro-mechanical systems, and other emerging technologies require the characterization of material behavior on length scales often as small as fractions of a micron. Recent advances in instrumented nanoindentation allow this technique to be used to accurately determine the mechanical properties of physical systems in these highly constrained volumes.

During nanoindentation, an indenter tip is brought into contact with the surface of the sample. A gradually increasing force is applied, and the displacement of the tip into the material is carefully measured to determine the deformation characteristics. Material deformation is initially elastic, as individual atoms move from their equilibrium positions; this displacement is completely recoverable when the stresses are removed. As the stresses increase, the sample eventually cannot sustain them elastically, and plastic deformation occurs. Plastic deformation corresponds to the generation and motion of crystalline defects within the solid, and is considered permanent. While this transition is often gradual in bulk materials, the onset of plastic deformation during nanoindentation is abrupt and relatively extensive, and is marked by a displacement burst of the tip into the sample. Although the displacement burst is a critical component of the behavior of materials on these length scales, the nature of the events involved is not well established. Current belief relates these events to the nucleation and multiplication of small numbers of dislocations in the region underneath the indenter tip, but without specifying a precise mechanism.

The recently available ability to generate and observe the motion of individual crystalline defects through nanoindentation is remarkable. This is a significant capability because nanoindentation allows the analysis of dislocation behavior when isolated from the enormous
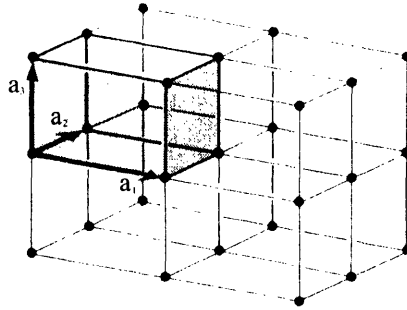
Figure 1: Tetragonal unit cell in a three dimensional lattice, with translation vectors given by a_1, a_2, and a_3 (after Kittel, 1996, p. 7) [1].

number of interactions among defects that occur during bulk deformation, and makes a fundamental understanding of dislocation nucleation far more accessible. Through these studies, a predictive model of dislocation nucleation may be reasonably developed. The increased control of physical properties in micron-scale systems that this allows is of substantial practical importance to the development of material systems for emerging applications, and is certainly a worthwhile field of applied physics in which to conduct research.

.

1.2   A BRIEF REVIEW OF CRYSTALLINE STRUCTURE[1]

Of the numerous classes of materials studied by solid state physics, crystalline solids are among the simplest to describe; an ideal crystal is an infinite, periodic array of atoms or groups of atoms. Compared to amorphous solids or real crystals, the periodicity of an ideal crystal simplifies its description enormously. The entire structure may be generated by specifying a single repeating element, known as a unit cell, and providing instructions for how to repeat that unit by a set of translation vectors. The process is begun by placing a single unit cell in a three-dimensional space, and using the translation vectors to repeat the cell in the specified distances and directions. Each one of the repeated unit cells is identical to the first, and is then duplicated using the same set of translation vectors. Continuing this process creates an ideal, infinite three-dimensional crystal. While many unit cells may be chosen for a given crystalline solid, convention dictates that the

---

[1] Although crystallography is an extensive field, what follows will be an abbreviated and selective treatment. Those with further interest are encouraged to refer to texts on materials structure [2, 3].

14
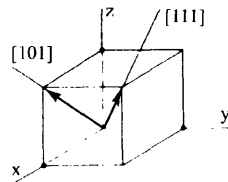
Figure 2: Directions in a cubic unit cell and relevant coordinate system. The [111] and [101] directions are depicted. (after Reed-Hill and Abbaschian, 1994, p. 14) [3].
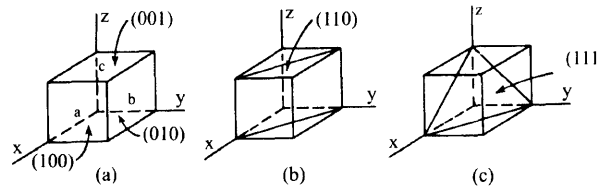
Figure 3: Planes in a cubic unit cell. (a) Faces of the unit cell: a(100); b(010); c(001). (b) The (110) plane. (c) The (111) plane (after Reed-Hill and Abbaschian, 1994, p. 16) [3].

smallest unit that still exhibits most of the symmetry of the complete crystal be used. An example of a simple unit cell and a segment of the crystal generated by that unit cell appear in Figure 1.

1.2.1 MILLER INDICES

Crystallographers usually describe unit cells through the use of Miller Indices, which provide a convention for identifying specific elements using numerical indices. For cubic unit cells, three mutually perpendicular edges of are taken to be the coordinate axes in a Cartesian coordinate system. The axes measure length in units of the lattice parameter, or the length of an edge of the unit cell; this normalizes the length of each edge to one.

Vectors in the unit cell may naturally be expressed in terms of their components parallel to the coordinate axes. However, given that an ideal crystal is infinite in extent and the features of a particular unit cell are periodically repeated, directions are often more useful in describing aspects of crystalline structure than are vectors. Convention dictates that the direction parallel to the vector $h\hat{x} + k\hat{y} + l\hat{z}$ be specified by a set of three coordinates, as [hkl]. Notice the use of brackets. Examples of common directions within the unit cell and the relation of these directions to the coordinate axes appear in Figure 2.

A system to describe planes within the unit cell is useful as well. Generally speaking, a plane with intercepts at 1/A, 1/B, and 1/C on the x, y, and z axes, respectively, is defined by the equation $1 = Ax + By + Cz$. Providing these intercepts allows the equation of the plane to be determined and the plane uniquely identified. Alternatively, the equation for the plane may be recast into the form $1 = x/h + y/k + z/l$, with the intercepts expressed as h, k, and l for the x, y, and z axes, respectively. A particular plane is then specified in terms of the intercepts, as (hkl).

15
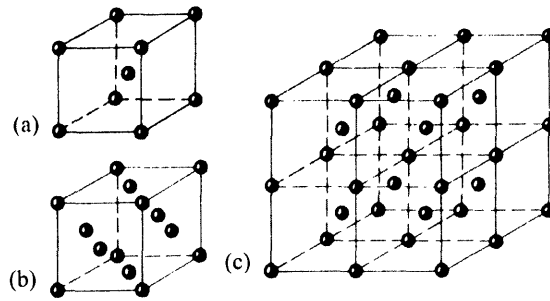
Figure 4: Crystalline cubic unit cells. (a) Body-centered cubic unit cell. (b) Face-centered cubic unit cell. (c) Segment of a body-centered cubic lattice (after Reed-Hill and Abbaschian, 1994, p. 5) [3].

Notice the use of parentheses. An interesting feature that follows directly from the preceding equations is that the direction [hkl] is perpendicular to the plane (hkl). Examples of commonly used planes appear in Figure 3.

1.2.2   ORDERED PACKING

One of the easiest ways to visualize the various possible cubic unit cells is to approximate the atoms as hard spheres, and to place these spheres at specified locations in a cube. The simplest possible cubic unit cell, known appropriately enough as a simple cubic unit cell, is a cube with a single, identical atom placed at each of the eight corners. While this structure is straightforward, few pure metals adopt a simple cubic structure. The formation of bonds between neighboring atoms reduces the enthalpy of the crystal, and therefore atoms tend to arrange themselves in structures that have a higher packing fraction than the simple cubic structure, in the sense of the fraction of total volume occupied by atoms.

A slightly more complicated unit cell is the body-centered cubic unit cell, and is referred to frequently as the BCC unit cell. This places an additional atom in the center of the unit cell, and may be seen in Figure 4(a). A number of pure metals adopt this structure at room temperature, due to the higher packing fraction and extent of local bonding.

A third cubic unit cell, and the one that will be of primary importance here, is the face-centered cubic unit cell, or the FCC unit cell. The FCC unit cell, which appears in Figure 4(b), has atoms on each of the eight corners, as in a simple cubic unit cell, and an additional atom in the

16

center of each of the six faces. One of the notable features of the FCC lattice is that this structure is the most efficient packing of identical spheres possible in three dimensions, and many pure metals adopt this structure at room temperature.

1.3   CRYSTALLINE DEFECTS

Although their description is rather elegant, perfect crystals do not exist in nature; that is, they do not exist at ambient temperatures. As thermodynamic systems, crystals tend to migrate toward the minimum in free energy, $G \equiv H - TS$, where H is the enthalpy, T is the absolute temperature, and S is the entropy of the system. Since enthalpy is reduced by the formation of atomic bonds, the enthalpy of the crystal is minimized in a perfectly ordered state, where each atom forms as many bonds as possible with its neighbors. At temperatures that are low enough to allow us to neglect the effect of the entropy term on the free energy, the perfectly ordered state of minimum enthalpy corresponds to the thermodynamic equilibrium of the crystal.

As temperature increases, the entropic term in the free energy becomes increasingly important. Suppose that the introduction of a defect into the crystal is associated with an entropy increase of ΔS and an enthalpy increase of ΔH. When the entropic change in the free energy $-T\Delta S$ outweighs the enthalpic change ΔH, the change in the free energy ΔG of the crystal resulting from the introduction of a defect is favorable, and imperfections become features of the crystalline solid. These imperfections, or defects, in the structure take on a number of forms, which are most easily classified by their dimensionality.[2]

1.3.1   POINT DEFECTS

One-dimensional imperfections, otherwise known as point defects, occur as either vacancies or interstitials. A vacancy is the absence of an atom from a location where one would be expected in an otherwise perfect crystal, as seen in Figure 5(a). An interstitial, on the other hand, is simply an

---

[2] The description of defects in this section is strictly limited to crystals containing atoms of a single element.

17
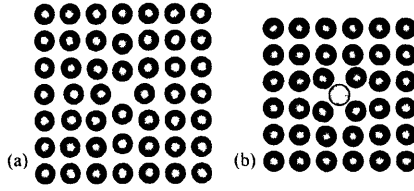
Figure 5: Crystalline point defects. Notice the local lattice distortions necessary to accommodate the defects. (a) Vacancy in an otherwise perfect crystal. (b) Interstitial in an otherwise perfect crystal (after Allen and Thomas, 1999, p. 252, 256) [2].

extra atom placed somewhere within the crystal. This is seen schematically in Figure 5(b). Notice that in Figure 5, the crystalline lattice locally distorts to contain the point defects. This behavior suggests that vacancies are attracted to regions of high compression, where the crystal lowers its overall energy by locally expanding into the available volume. Near an interstitial on the other hand, the crystal compresses. Interstitials consequently experience a net attractive force towards regions of high expansion, where the crystal lowers its overall energy by locally compressing. Further note that the migration of an interstitial onto a site occupied by a vacancy cancels the local distortion fields and leaves the crystal once more in a locally perfect configuration.

The number of vacancies within a solid is generally measured at equilibrium as a fraction of the total number of available sites. Represented by x_v, this value is determined from statistical thermodynamics to follow the equation

$$x_v = \exp\left(\frac{\Delta s_v}{k}\right)\exp\left(-\frac{\Delta h_f}{kT}\right)$$

(1.1)

where k is Boltzmann's constant and T is the temperature of the crystal in Kelvin[3]. Δh_f and Δs_v represent the activation enthalpy of vacancy formation and the vibrational contribution to the entropy for vacancy formation, respectively. For platinum, the experimentally determined values for these quantities are 1.4 eV and 2.9 k_B, respectively [4]. The equilibrium frequency with which interstitials occur in a solid is given by a relation similar to that for vacancies, except that the activation enthalpy for interstitial formation and the vibrational contribution to the entropy for interstitial formation are used instead.

---

[3] For a derivation of this result , see Appendix A.

18

1.3.2 LINE DEFECTS

Line defects, otherwise known as dislocations, strongly influence the deformation behavior of crystalline solids. To observe this, notice that by employing a mechanism where planes of atoms slide past one another, a perfect crystal should theoretically be able sustain a shear stress up to about one sixth of the shear modulus of the material without permanently deforming; that is,

$$\tau = \frac{1}{2\pi} \mu \tag{1.2}$$

where τ is the theoretical shear strength, and μ is the shear modulus of the crystal [3]. Experimentally, crystals are observed to deform plastically in bulk at stresses on the order of one ten-thousandth of the theoretical shear strength. The reason for this substantial difference in behavior is the presence of dislocations within the real crystal.

During bulk deformation, the crystalline sample is observed to deform by sliding one part across an adjacent part, referred to as slip. The plane on which slip occurs is the slip plane, and is a characteristic of the structure of the lattice. Generally, the slip plane corresponds to the closest-packed plane, or the plane in which the atoms are most densely packed. For BCC and FCC crystals, this means that the slip planes are similar to the (110) and (111) planes, respectively. These closest-packed planes are preferred simply because the distance required for atomic planes to travel between stable points is shortest. Similarly, the direction of slip within the slip plane tends to be the direction of closest atomic packing. As a set, the preferred directions and planes for slip within a crystal are known as the preferred slip system.

The mechanism of deformation by dislocation motion is essentially the discretization of the deformation into line segments within the crystal, each of which transmits a displacement on the order of a single atomic spacing. These line segments, or dislocations, travel through the lattice under an applied shear stress, as depicted in Figure 6. As the dislocation migrates, an overall sliding of one part of the crystal relative to an adjacent part is developed, but by using only a local process of bond breakage and reformation to transfer the dislocation incrementally through the lattice. The energy requirements for this localized process are much more modest than for the mechanism used to determine the theoretical shear strength, as revealed by the difference in the theoretical and observed behaviors.

19
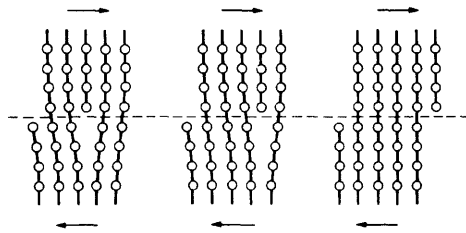
Figure 6: Edge dislocation motion through a two dimensional lattice under an applied shear tending to move the upper surface to the right (after Kittel, 1996, p. 591) [1].

The unit of displacement that is carried by a dislocation is known as the Burgers vector, is a vector quantity, and is identical at every point on the dislocation. The magnitude of the Burgers vector effectively measures the strength of the dislocation, and is usually approximately the distance between atoms in the closest-packed direction of the closest-packed plane. In the case of platinum, this is around 2.78 Å. A dislocation is completely specified by the Burgers vector and by the unit vector that locally points in the direction of the dislocation line. For the dislocation to be mobile, that is, to be able to transmit the unit of deformation to a different region of the crystal, the Burgers vector and the dislocation line must lie within one of the available slip planes.

Dislocations may be classified as one of several types, based on the relative orientation of their Burgers vector and dislocation line. When the Burgers vector is perpendicular to the dislocation, the result is known as an edge dislocation. This type of dislocation is visible in Figure 7(a), where the Burgers vector of the dislocation is parallel to the x axis and the dislocation core is parallel to the z axis. The structure of the edge dislocation effectively corresponds to the insertion of an additional half-plane of atoms, and the core of the dislocation runs along the edge of the inserted half-plane. Notice that because the edge of the plane of atoms cannot end abruptly within the crystal, neither can the dislocation line. This is in fact a specific case of a more general result, that dislocation lines only end on dislocations or other higher-order defects.

When the Burgers vector of the dislocation is parallel to the dislocation line, the result is known as a screw dislocation. A segment of one such dislocation appears in Figure 7(b), where the Burgers vector and the dislocation core are parallel to the z axis. This structure is referred to as a screw dislocation because successive circuits constrained to the crystalline lattice that travel around the dislocation core follow a path through the crystal similar to the threads on a screw. A final type of dislocation, known as a mixed dislocation, has a Burgers vector that is neither
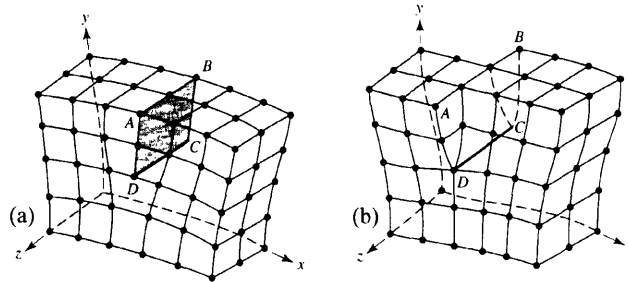
Figure 7: Dislocations in a primitive cubic lattice. (a) Edge dislocation segment. (b) Screw dislocation segment (after Allen and Thomas, 1999, p. 276) [2].

perpendicular nor parallel to the dislocation line, and displays characteristics intermediate between those of an edge dislocation and a screw dislocation.

One characteristic of dislocations is that the highly local deformation of a dislocation gives rise to substantial long-range stresses, meaning that they interact and react with each other over long distances to form arrays or larger structures. For example, a single dislocation may dissociate into smaller dislocations that then travel independently, or several dislocations may join to form a single dislocation with an overall Burgers vector given by the vector sum of the individual ones. Notice that dislocations with equal and opposite Burgers vectors generate attractive stress fields. When such dislocations meet, they annihilate and leave behind a locally perfect crystal.

Dislocation nucleation is a different matter; the specifics of the event differ substantially depending on the conditions of nucleation. Any dislocation generated through a process involving some defect or heterogeneous component of the crystalline structure is referred to as a heterogeneously nucleated dislocation. Bulk deformation processes generally involve heterogeneously nucleated dislocations, since the stressed volume is extensive enough that the chance of interacting with a heterogeneous nucleation site is high. The external stresses required to nucleate a dislocation through this mechanism are comparatively small, since large internal stresses and stress concentrators around heterogeneous sites encourage dislocation nucleation. On the other hand, dislocations may be nucleated within a perfectly crystalline region, through a process of homogenous dislocation nucleation. These must take the form of dislocation loops, with the same Burgers vector at each point. Although the earliest stages of homogenous nucleation are not well understood, relatively large shear stresses, on the order of the theoretical

21

shear stress, seem to be necessary. Once the loop is nucleated, much smaller shear stresses are sufficient to make the loop rapidly expand. The homogenous nucleation of dislocation is usually observed only with the application of high shear stresses to limited volumes.

1.3.3   HIGHER ORDER DEFECTS[4]

While many higher-dimensional structures may be considered to be defects, only a few of these structures appear in most crystalline solids. One of these occurs simply because crystals must be finite in extent; although a perfect crystal extends infinitely in every direction, real crystals must end on a free surface. The properties of the crystal on the surface often differ markedly from the bulk characteristics, for example, with regard to phonon propagation or binding energies. Nevertheless, since the fraction of the total crystal near the surface is usually small, the bulk properties of the crystal usually provide a reasonable approximation to the overall character. One of the most notable features of a free surface is that this structure provides a source for vacancies, interstitials, and dislocations to migrate into the solid.

Grain boundaries may be considered as an extension of the concept of the finite nature of a crystal. Rather than a free surface though, a grain boundary is the border between separate crystals with distinct orientations. Given that most crystalline materials are much larger than the individual crystals from which they are composed, grain boundaries usually occur much more frequently within crystalline materials than free surfaces. They therefore have a correspondingly greater effect on the properties of the solid. As with free surfaces, grain boundaries provide sources and sinks for other crystalline defects that may arise in response to mechanical deformation or thermal fluctuations.

---

[4] Often, higher-dimensional elements of the microstructure are considered to be characteristics of the crystalline solid rather than defects.

1.4   STATE OF THE ART IN NANOINDENTATION

As applied physics approaches the nanoscale, the understanding of the fundamental mechanisms underlying fracture and plasticity becomes increasingly desirable and achievable. Material properties on these scales tend to differ markedly from their bulk counterparts due to the remarkably small volume of material involved, and manipulation of these unusual properties may result in various substantial breakthroughs in material performance. The pertinent mechanisms appear to behave on the scale of nanometers. Due to recent advances in instrumented nanoindentation that permit continuous monitoring of the load and depth of the indenter tip to angstrom-level depth resolution and nanonewton-level force resolution, nanoindentation provides a convenient means to investigate properties on this scale. During nanoindentation, an indenter tip is brought into contact with a sample of material and penetrates the surface until a specified load or depth is reached.

Displacement of the indenter tip initially corresponds to elastic deformation of the surface, where the initial strain of the sample is completely recoverable [5-20]. As the applied force increases, the stresses eventually become large enough that the crystal must deform plastically, or irrecoverably, to accommodate them. This onset of fully plastic behavior during nanoindentation is generally observed to coincide with a displacement excursion during load controlled nanoindentation, and a load drop during displacement controlled nanoindentation [5-16, 18, 21-30]. Figure 8 gives a typical nanoindentation load-displacement curve, with the initially elastic region and subsequent plastic region clearly marked. Although the deformation of bulk materials includes similar elastic and plastic regimes, the current behavior differs from that of bulk samples in at least one important respect; the shear stress sustained by the crystal during nanoindentation before plastic failure is on the order of the theoretical shear strength of the crystal [7, 10-13, 15, 16, 18, 19, 22, 24, 26, 28-31]. Shear stresses of this magnitude immediately suggest a mechanism dependent on homogenous dislocation nucleation, as has been directly observed in simulations under a variety of conditions [21-24, 32] and implied by numerous experimental studies [7, 9, 14-16, 21-25, 32, 33]. This appears to be reasonable given the small probability of finding a heterogeneous nucleation site within this highly constrained volume [9], and is substantiated by observations of significant changes in the hardness or stiffness of the indenter material during and after plastic yielding [10, 11, 16, 34].

23
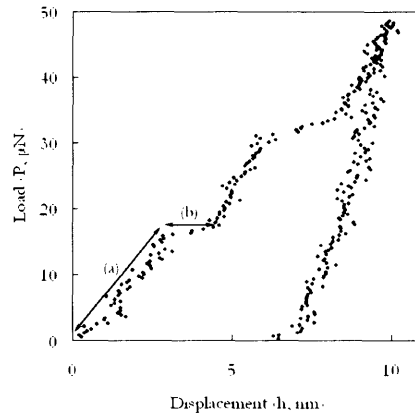
Figure 8: Example of a load-displacement curve for nanoindentation into (110) oriented single-crystal platinum at 25°C with a loading rate of 250 μN s^{-1}. Region (a) is elastic, and the initiation of plasticity occurs in Region (b).

The initial elastic deformation of the sample is now recognized as being well described by Hertzian contact mechanics, which are used to calculate the elastic deformation and stress state of the material underneath the indenter tip[5]. This observation has been experimentally verified for a variety of materials and surface conditions; for example, during the simulated indentation of a Au single crystal [24], for experimental indentation into Au covered with a passivating surface monolayer [7, 19, 20], during the elastic indentation of bulk metallic glasses [17], and for numerous other surfaces [5, 13-15, 18, 26, 36].

1.4.1   EXPERIMENTAL NANOINDENTATION

Meanwhile, some dispute over the nature of the displacement excursion during the onset of plasticity still exists. Although the precise mechanism seems to be system dependent, one of two basic phenomena appears to be responsible in nearly every case; the observed displacement burst is either related to the indenter tip breaking through a surface oxide layer, or to the direct nucleation and multiplication of dislocations in the crystalline region underneath the indenter tip. When the latter mechanism is active, the displacement excursion is frequently known as a pop-in.

---

[5] Refer to Introduction to Contact Mechanics [35] for a further discussion of Hertzian contact mechanics.

The main factor determining the active mechanism for a particular system is simply the presence or absence of an oxide layer of sufficient thickness.

A number of experimental nanoindentation studies centered on investigating and developing an understanding of the oxide breakthrough mechanism, and particularly the events leading up to breakthrough. The current understanding models the oxide layer as a hard plate or membrane on the surface of the substrate. During the initial stages of indenter tip loading, the substrate and the oxide deform elastically in a manner similar to Hertzian elastic theory [12, 13, 18, 37]. The harder oxide reduces the stresses experienced by the substrate by distributing the indenter force, through the plate-bending and membrane-stretching effects [37]. Increasing the applied load results in elasto-plastic deformation of the substrate and dislocation nucleation beneath the indenter, although much of the force is still supported by the oxide [12, 13, 18, 26, 37, 38]. Eventually, loading causes dislocation multiplication within the solid, failure of the oxide film by cracking or fracture, and the onset of fully plastic deformation by a displacement excursion [12, 13, 26, 37, 38]. Notice that in this case, the dislocations may be nucleated before the displacement excursion, and that dislocations involved in the excursion may be heterogeneously nucleated. This mechanism is strictly limited to materials with an oxide though, and does not necessarily pertain to the onset of plasticity in other materials.

During investigations into oxide breakthrough, several variables that influence the behavior of the material near a displacement excursion became apparent. For example, the momentum of the indenter tip on contact with the surface substantially alters subsequent plastic behavior. High initial momentum of the indenter tip may deform asperities or other surface irregularities and generate defects on contact, thereby reducing the future stress necessary to fracture the oxide. Indentations with small initial momentum only generate defects that lead to oxide fracture after the initial contact, at a more predictable point in the loading cycle [34, 39]. Alternatively, asperities or surface steps may encourage dislocation nucleation through stress concentrating effects [27, 38]; use of an atomically flat sample surface reduces this possibility.

Performing nanoindentation on metallic surfaces without a native oxide layer presents more difficulties than might initially be expected. Many clean metallic surfaces rapidly form oxides under ambient conditions, especially at elevated temperatures, and these samples must be isolated from possible sources of oxygen during indentation. Other challenges arise when a metallic indenter tip is used; during the approach of clean metal surfaces, the phenomenon of a jump-to-

contact is frequently observed. This is driven principally by the tendency of metallic surface atoms to form bonds and thereby reduce their surface area, and results in immediate plastic instabilities [19, 40, 41]. Studies of pop-in behavior related to homogenous dislocation nucleation and subsequent multiplication on oxide free surfaces therefore rely on indentation into ceramics [8, 16] or specifically prepared metallic samples [7, 19, 20].

As with studies of displacement excursions in metals covered by an oxide, nanoindentation studies into these more specific systems identified several system parameters critical to the pop-in behavior of the substrate. For instance, the radius of the indenter tip was found to substantially affect the maximum shear stress sustainable by the lattice before plastic deformation. This seems to be one component of the phenomenon known as the indentation size effect, where the extent of loading during indentation influences the mechanical properties of the sample [20]. More often, the indentation size effect refers to the observation that the hardness begins with a surprisingly elevated value, falls sharply with increasing load, and gradually approaches the bulk value [6, 11]. Some insight for this source of this effect comes from observations of the generalized plastic response of the contact volume, and particularly the configuration of the local dislocation network [6, 16, 42-48]. Given the action of a dislocation nucleation and glide mechanism, the slip planes available in the region of the indentation determine the direction of propagation of the dislocations and the resulting geometry of the residual indentation as well. This effect is manifested as a dependence of the indentation characteristics on surface orientation, and may be compounded by elastic anisotropies of the indented material [7, 15].

Other complicating behaviors include the involvement of unexpected modes of plastic deformation in certain ceramic crystals, including twinning [8], cracking [16], and phase transformations [16]. Analysis of acoustic emissions during indentation into crystalline ceramics indicates that variations in sample orientation or loading rate may actually change the mechanism involved in the initiation of plastic behavior, and that multiple mechanisms may be simultaneously active [8]. Examinations of energy dissipation mechanisms at elevated temperatures found heavy involvement of point defect migration in the transfer of mass from the indentation site, but for applied loads outside of the range usually considered as nanoindentation [43, 46-49].

1.4.2 SIMULATED NANOINDENTATION

Simulations of nanoindentation experiments offer several advantages over experimental studies; the conditions of the indent are much more precisely controllable during simulations, and the local behavior of the material within the substrate during the indentation may be directly observed and analyzed. Despite these benefits, there remains some uncertainty concerning the accuracy of the methods employed, as evidenced by the differences in the values of material properties derived from simulations and experiments. Concerns may be raised, for instance, about the limited scale of the simulated nanoindentation experiments. While the resolution of experimental nanoindentation and the computational power available for simulated nanoindentation continue to increase, the scale of the two does not yet overlap. Performing simulations using the volumes of material sampled during experimental nanoindentation is simply computationally prohibitive. The resulting artificial restrictions on the size of the indented material, along with the frequently used techniques of periodic boundary conditions and fixed boundaries, may lead to elevated material strength or other spurious effects. This calls into question the usefulness of applying the results of such studies to the understanding of phenomenon seen during experimental nanoindentation.

One effect that may be related to limited sample size is an elevated value of the maximum resolved shear stress sustainable by a material before plastic deformation. As an example, several simulations of nanoindentation into Au detected maximum resolved shear stresses higher than 5 GPa [22, 31]. Meanwhile, the ideal shear strength of Au is experimentally estimated and theoretically verified to be around 2 GPa. The researchers suggest that the discrepancies may be explained by the fact that experimental nanoindentation probes only the average sustained stresses, and not the highly localized values of shear identifiable in simulations. With respect to other material properties, Fang *et al.* [50] found the hardness and Young's modulus from simulated nanoindentation of copper to be approximately 12 and 3 times the respective experimentally determined values.

While these elevated values may simply be an extreme instance of the indentation size effect, mounting evidence implies that the difference in hardness or shear strength of simulated thin films from the bulk samples is a spurious result of the methods employed during simulation. This appears to be due partly to a limited sample size artificially restricting the distance that dislocation structures or other defects are able to travel from the site of the indentation. A molecular

dynamics simulation of indentation into a comparatively large sample of silicon nitride, consisting of more than 10 million atoms, revealed that plastic deformation does indeed extend into regions far from the location of the indent [51]. Hardness values derived from this simulation for α-Si_3N_4 match the experimental values well, and lend some support to the notion that unwanted effects may be reduced or eliminated by expanding the size of the system. A further effect is apparently related to the properties of the bottom layer of simulated atoms, which are commonly fixed. As the thickness of simulated films decreases, the overall behavior increasingly reflects the properties of the fixed bottom layer [23, 24]. This elevates the values of the hardness and elastic modulus for the materials, and may influence other related quantities. Fortunately, departures from a strict molecular dynamics method allow the simulation of larger samples without appreciably increasing computation time [23, 32].

Limitations imposed on simulations due to system size may be compounded by the practical number of time steps able to be performed during simulation, as in a study by Yu *et al.* [52]. Although the authors expected to observe dislocation nucleation and migration, the restriction of the sample size seemed to favor point defect generation and migration over the formation of dislocations. Further complications arose from the local melting of the simulated Al sample due to the generation of heat from an artificially high indentation rate, on the order of 300 m s^{-1}. Simulations tend to use indentation rates much higher than nanoindentation experiments in order to limit the number of computational operations required per indent, but this indentation rate is unusually high even for simulations. The effect of this high indentation rate on the nucleation of dislocations, when they do nucleate, is not well understood.

Nevertheless, a variety of important conclusions have been found as a result of simulations, and especially as a result of the connections between experimental and simulated studies. A study recently made progress in explaining the physical mechanisms underlying the indentation size effect [23]. One simulation reported the mechanism of heterogeneous dislocation emission from grain boundaries, which is critical to the deformation of polycrystalline materials [24]. With regard to homogenous dislocation nucleation, the surface healing occasionally observed following the initiation of plastic deformation and the withdrawal of the indenter tip appears to be a real effect, and may occur as long as continued yielding of the substrate does not generate dislocation locks [31].

1.4.3 PROPOSED DISLOCATION NUCLEATION MECHANISMS

According to continuum mechanics, shear stress is the principal driving force behind plastic deformation. At the continuum level, the onset of plasticity by dislocation migration occurs when the shear stress on a glide plane exceeds the critical shear stress τ_c, as given by Schmidt's Law. This concept of a critical shear stress may naturally be extended to the case of homogenous dislocation nucleation, for which one criterion states that dislocations nucleate and glide on the available slip planes once the shear stress underneath the indenter reaches a critical value [9, 11, 13-15, 18-22, 24-26, 28, 31, 33]. Although this criterion is straightforward and intuitively appealing, some studies seem to challenge the underlying assumption that homogenous dislocation nucleation is completely shear controlled. Several 2D indentation simulations found that dislocation nucleation did not occur at the location of maximum resolved shear stress [23, 53]. While these do not completely capture the behavior of a real crystal, the presented results seem suggestive of a more complex yield criterion. Based on indentations into several different orientations of Au, Kiely and Houston [7] proposed a revision to the critical shear stress criterion, in which dislocation activity begins only once the shear stress in the crystal reaches a particular value on all available slip planes. Nevertheless, since they remained unable to identify the site of dislocation nucleation as experiencing the shear stress τ_c, a complete characterization of the phenomenon requires further study.

As with the criterion for the onset of plasticity, continuum mechanics provides a basis from which to develop an understanding of the mechanism of homogenous dislocation nucleation. Michalske and Houston [20], and Chiu and Ngan [14], employed a continuum mechanical description of the total energy of a dislocation loop based on the treatment of Hirth and Lothe [54] to determine the shear stress required to make dislocation nucleation energetically favorable. This model explains the dependence of the indentation size effect with respect to the radius of the indenter tip, but breaks down as the radius of the loop decreases and atomistics become increasingly important. Since a nucleating dislocation loop is expected to encompass only a few atomic volumes, the continuum level description of dislocation nucleation is not entirely appropriate.

Rigorous atomistic models for the homogenous nucleation of dislocations do exist. One of these, termed the Λ criterion by the authors, defines a tensor that describes phonon behavior

within the solid. For materials experiencing elevated stresses, certain frequencies of phonons may become unstable; the amplitudes of these phonons increase exponentially in time. Eventually, the magnitude of the wave exceeds the elastic limits of the solid, and a defect is homogenously nucleated. This may then provide a site for dislocation multiplication, and the onset of plasticity in the material. The Λ criterion predicts the site and the slip character of homogenously nucleated dislocations remarkably well for molecular dynamic simulations [30]. An alternative model, presented as the N criterion, predicts the site and character of a homogenous nucleation event as well as the Λ criterion, and is more theoretically robust. Rather than examining the stability of inherently local constitutive equations, the N criterion predicts material behavior based exclusively on thermodynamic considerations [53]. Neither of these models completely settles the issue of homogenous dislocation nucleation though. These criterions depend principally on theory and simulations for their support; although nucleation events may be directly observed and the values of the Λ and N criterion calculated for each point in a crystal during simulation, methods for applying these to experimental nanoindentation remain unclear. Aside from the formidable technical challenges of validating these models experimentally, they cannot account for experimentally observed changes in the indentation behavior with certain thermal or temporal characteristics of the indentation system.

Mounting evidence points to the influence of elevated temperature on deformation response during nanoindentation, but for the most part without offering satisfactory explanation of the behavior. The research group of Ngan [21, 55] performed a number of molecular dynamics simulations on highly constrained systems. These traced the homogenous nucleation of dislocations back to the formation of small atomic clusters, even on the scale of a single atom, with an elevated concentration of thermal energy and high relative displacement to the surrounding region. Nevertheless, seeing as an eventual nucleation site may always be traced back to an arbitrarily small area, these findings do not reflect the critical size necessary to form a stable dislocation loop, and offer no further insight into the homogenous dislocation nucleation process. Several simulations, one by Yu *et al.* [52] and one by Fang *et al.* [50], allowed temperature to vary during nanoindentation. They only concluded that the indented material becomes softer with increasing temperature, as is expected from bulk behavior. These simulations did not appreciably advance understanding of the effect of temperature on the mechanism of dislocation nucleation, since effects resulting from system size limitations and geometric considerations apparently

favored point defect generation over dislocation nucleation. A few experimental studies suggest that thermal activation may participate in the process of homogenous dislocation nucleation, but without outlining a descriptive theory [10, 16, 28]; experimental observation of thermal effects is limited to the determination that elevated temperatures encourage plastic behavior [38]. This difficulty is probably related to the extreme sensitivity of nanoindentation equipment to thermal drift, and difficulty in thermally isolating the nanoindentation device.

Meanwhile, investigations have been conducted into a variety of observable, time dependent indentation behaviors, but the explanations offered for these are frequently minimal. A certain type of experiment is known as a holding experiment, where a constant sub-critical load is applied to the surface and a displacement burst is observed to occur after a varying holding time. The dependence of the critical event on time is explicit in these experiments, since the holding time required to observe a displacement burst increases rapidly with decreasing load [14, 15, 33, 38]. On a related note, the presence of asperities near to the indentation site appears to have a weakening effect on the time dependent properties of metallic surfaces during holding experiments [38]. Alternatively, a time dependence may be introduced by changing the rate of load application during indentation. Study of this phenomenon is limited to the observation that increasing the loading rate appears to increase the critical load for pop-in [15]. Unfortunately, these studies for the most part neither adequately characterize the time dependence, nor relate the time dependence directly to a nucleation mechanism.

An emerging school of thought suggests that the temperature of the sample and the time dependent properties of the onset of plasticity are closely related. Suppose that the reported ranges in critical load reflect the action of an inherently stochastic process, rather than variability in the condition of the surface or other sources of experimental error. This implies a probabilistic, thermally-activated nucleation event. Several groups theorized that this reflects a mechanism of vacancy climb, which would allow a dislocation loop to expand by a process of point defect absorption, until the loop expands beyond a critical size [14, 15, 56]. Considering the significant number of vacancies this type of mechanism would require, point defects would need to migrate to the location of the incipient dislocation loop. A Maxwell-Boltzmann distribution in thermal energies renders room temperature vacancy migration extremely unlikely though, given activation enthalpies on the order of 1.4 eV for platinum [4]. Mechanisms involving vacancy climb therefore needs further development to provide viable explanations for the nucleation process.

31

Bahr *et al* [33] performed a series of holding experiments, and found that of several conceivable mechanisms, only dislocation loop nucleation matched the experimentally observed load dependence of the holding time until yield. To explain the time dependence, he proposed an attempt frequency for homogenous dislocation nucleation, and an initial energy barrier that must be overcome for yielding to occur. The contribution of thermal effects implies a rate of dislocation nucleation of the form

$$\dot{N} = \eta_0 \exp\left(-\frac{\Delta G}{kT}\right) \tag{1.3}$$

where ΔG is the energy barrier to dislocation nucleation and η_0 is the attempt frequency [33, 54]. While this model acceptably captured the load dependent behavior of the holding experiments, an attempt to probe the rate dependence on temperature over a limited temperature range remained inconclusive.

Further investigation into the nature of the pop-in as a probabilistic, thermally-activated nucleation event refined the form of the expression for nucleation rate, and provided experimental evidence for the validity of this description. Rather than using a description of the energy barrier derived from continuum mechanics, the research group of Schuh expressed the energy barrier ΔG as an activation enthalpy reduced by a shear stress-bias acting over the relevant volume, yielding the expression

$$\dot{N} = \eta_0 \exp\left(-\frac{\varepsilon - \tau v}{kT}\right) \tag{1.4}$$

where ε is the activation enthalpy, τ is the shear stress local to the nucleation site, and v is the activation volume [5, 36]. Since this formulation assumes less about the initial event than the corresponding continuum mechanical expression, the experimental values of the activation enthalpy and the activation volume may be used to determine the specific nature of the onset of plasticity. Experiments investigating the dependence of the critical load distribution on loading rate followed the prediction of Equation (1.4), and provided an activation volume of 4.6 $\mathring{A}^3$ for silicon carbide [5]. Employing the same model, Wo *et al* [55] found an activation volume of 24 $\mathring{A}^3$ for Ni$_3$Al. These values indicate that the pop-in mechanism, believed to be the homogenous nucleation of dislocations, may initially be related to the behavior of a single atomic volume. With respect to the activation enthalpy, indentations performed by the Schuh group over an expanded temperature range, from 20°C to 200°C, revealed an explicit temperature dependence of the

nucleation rate, but without sufficient sampling to determine a precise enthalpy value [5]. Further experimentation that varies the sample temperature may permit the activation enthalpy to be determined, and significantly advance the understanding of incipient plasticity during nanoindentation.

CHAPTER 2

THE EXPERIMENT

2.1   THE DISLOCATION NUCLEATION QUESTION

The phenomenon of pop-in is receiving intense scrutiny from the applied physics and materials science communities, visible by the extent of research conducted within recent years. Due to advances in experimental resolution and computational power, this research may be conducted either through nanoindentation experiments or simulated nanoindentation. Although the scales of these techniques nearly overlap, the aims of experiments and simulation within the literature differ significantly. Simulations often attempt to harness the directly observable motion of individual elements of the system to develop models for the onset of plasticity during nanoindentation. Spurious, unphysical effects introduced by the type of computational model employed, or the inapplicability of the resulting models to experimental nanoindentation, often hamper the results of simulations though. Meanwhile, experimental investigations frequently identify factors that may be involved with the pop-in phenomenon, but theoretical explanations continue to be minimal.

The understanding of the pop-in phenomenon as controlled by a stochastic, thermally-activated, stress-biased event is only a recent development. This nevertheless represents a significant achievement toward the development of a predictive model for the onset of plasticity in controlled volumes. The formulation of this concept by Schuh *et al.*, captured in essence by Equation (1.4), is particularly useful since this allows the nature of the pop-in event to be determined from experimental results. An extensive and statistically significant sampling of indentations under various loading rates and temperatures could therefore, through the proper analysis, establish the characteristic activation enthalpy and attempt frequency of the dislocation nucleation event in a physically realistic system for the first time.

2.2   EXPERIMENTAL METHODS

From the discussion of the nanoindentation literature, a number of experimental factors are identified that sharply alter the indentation behavior of a material and shift the statistics for the onset of plasticity. This section describes the specifics of the indentation process, and the attempts to either reduce the influence of these effects or systematically control them to probe the nature of the displacement excursion. These considerations may be divided into three broad categories. The details of the choice of sample type and the sample preparation are outlined. Then, the specifics of the indenting device and modifications to the device are described. The section on the identification of pop-in events provides a reasonable transition into the description of the mathematical methods employed.

2.2.1   SAMPLE PREPARATION

Goodfellow (Berwin, PA) provided several oriented platinum single crystal samples of 99.999% purity. The absence of an ambient oxide layer on platinum eliminated numerous potential complicating factors, including the distribution of the applied load over a large area of oxide and the heterogeneous emission of dislocations from the oxide-metal interface. Meanwhile, the use of a pure metal with a face-centered cubic crystalline structure, in which the Burger's vector of dislocations is clearly specified and dislocation motion is restricted to the glide planes, significantly simplified the analysis of dislocation nucleation and glide within the material.

Sample preparation before indentation entailed embedding the samples in an epoxy mount and mechanically polishing the surface using sequentially finer silicon carbide paper and diamond pastes, down to a final mechanical polish with 0.1 μm diamond paste. Mechanical polishing of surfaces introduces a high surface dislocation density, and reduces the stresses required for the onset of plasticity [10, 12]. Therefore, the samples were electropolished in a supersaturated solution of 100 ml H_2O, 25 ml HCl, and 40 grams of NaCl for 2 minutes at a potential of 4.0V DC with a copper electrode, to remove the deformed surface layer and reduce the surface roughness. This procedure was followed by one more mechanical polish with 0.1 μm diamond paste, and a further electropolish under the same conditions. The result of this preparation was that when

examined under the AFM, the sample surface had a rms roughness of less than one nanomenter, and could be reasonably approximated as an elastic half-volume as is assumed in Hertzian contact mechanics. Given this value of the surface roughness, asperities or steps must only appear infrequently on the surface.

Before insertion into the indenting device, the epoxy mount surrounding the samples was dissolved and the polished samples were recovered. Each sample was then mounted to a stainless steel, magnetic AFM metal specimen disk, as provided by Ted Pella (Redding, CA), using J-B Weld, an epoxy provided by the J-B Weld Company (Sulphur Springs, Texas). The elastic moduli of the specimen disk and the epoxy were sufficiently high that the observed deformation may be considered effectively restricted to the sample, without any compliance from the mount; during indentation, the load applied to the sample is effectively distributed over the entire contact area between the sample and the epoxy, reducing the stress on the epoxy to negligible levels.

2.2.2   EXPERIMENTAL SETUP

Nanoindentation was performed using a Hysitron Triboindenter, commercially available from Hysitron Inc. (Minneapolis, MN). One of the benefits of using this setup is the ability to scan the surface using AFM without removing the sample from the Triboindenter enclosure, allowing the immediate imaging of indentation sites. The published specifications for the transducer assembly, which is the portion of the indenter directly responsible for applying the load and measuring the resulting displacement of the indenter tip, indicate a load resolution of 1 nN and a displacement resolution of 0.04 nm. Due to slight mechanical vibrations, the transducer assembly attained a practical resolution somewhat larger than these values, but nevertheless remained well below the scale of the indentations performed. The indenter used was a Berkovich diamond tip commercially available from Hysitron, with an effective tip radius of about 150 nm as determined by fitting the elastic loading portion of indentations into silicon carbide to the Hertzian elastic prediction [5]. The determination of the tip radius from fitting the Hertzian elastic contact model to the elastic loading portion of nanoindentation curves is an accepted technique, and is performed regularly in the literature [5, 6, 17, 19, 20, 33, 36].
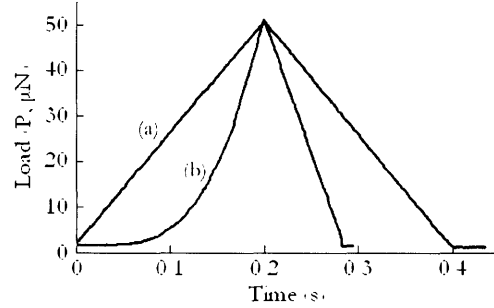
Figure 9: Loading functions used for indentation. (a) Constant change of load in time during loading and unloading. (b) Constant change of maximum shear stress beneath the indenter in time during loading, and constant change in load in time during unloading. Notice the initiation of loading from the baseline contact force of 2 μN.

Variables in the indentation procedure included the sample orientation, the form of the loading function, the loading rate, and the temperature of the system. Indentation was performed on three samples, with exposed indentation surfaces parallel to the (100), (110), and (111) crystallographic planes. Characterization of the indentation behavior for multiple orientations was meant to establish whether a single pop-in mechanism was active for every material orientation. Similar to indentations performed into Au, the (100) oriented sample sustained much smaller stresses before deviation from Hertzian elastic behavior than the (110) or (111) samples, due to the differences in the available slip planes and elastic anisotropies of the solid [7]. Regrettably, the pop-in loads for the (100) sample proved to be small enough that meaningful results could not be obtained for that orientation.

The Hysitron Triboindenter allows indentations to follow any loading curve as a function of time, denoted by P(t), assembled from a collection of line and sinusoidal segments. The loading functions used during this study appear in Figure 9. The function in Figure 9(a) increases the external load at a constant rate up to the peak value, and then decreases the load at a constant rate. The function in Figure 9(b) increases the maximum shear beneath the indenter at a constant rate until the external load reached the peak value, and then decreases the load at a constant rate. Hertzian elastic theory specifies that the maximum shear stress τ_{max} beneath the indenter is given by

$$\tau_{max} = \frac{0.47}{\pi} \cdot \left(\frac{4E_R}{3R} \right)^{2/3} \cdot P^{1/3},$$

(2.1)

37
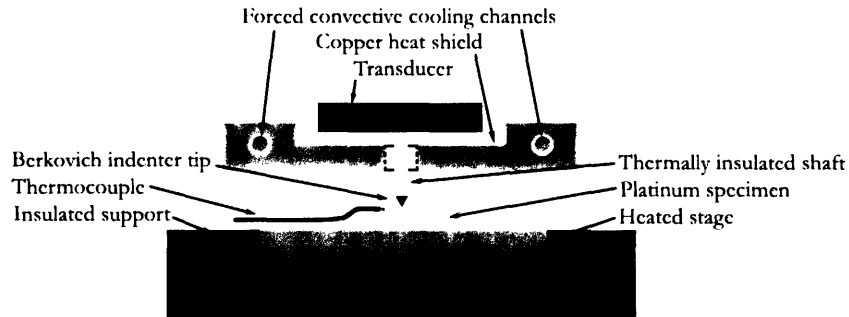
Figure 10: Schematic of the sample stage, indenter assembly, and
thermal equipment of the modified Hysitron Triboindenter.

where R is the radius of the indenter tip, P is the external load, and E_R is the reduced modulus as in Equation (B.3) [6]. This equation implies that to increase maximum shear stress at a constant rate, the loading function must increase the applied load as the cube of time, as in Figure 9(b). Each indentation reached a maximum load of 50 μN. The time to reach maximum load was varied between 0.02, 0.06, 0.2, 0.6, and 2 seconds; these loading times for the function in Figure 9(a) may equivalently be referred to in terms of the rate of load application, or 2500, 833, 250, 83 and 25 μN s^{-1} respectively.

The ability to perform indentations at elevated temperatures, up to 200°C, required the use of a modified, commercially available heating stage. As the transducer is extremely susceptible to thermal drift, the unit was thermally isolated from the heating stage by use of a low thermal-conductivity indenter shaft and a copper shield cooled by forced convective channels. A J-type thermocouple was used to monitor the temperature of the transducer, and ensure that it did not see elevated temperatures. The temperature of the sample was monitored through use of a J-type thermocouple bonded directly to the sample surface. To ensure that the temperature reading accurately reflected the state of the sampled volume, and that the sampled volume did not interact with dislocation structures generated by previous indents, indentations were performed within 2 mm of the thermocouple probe tip and at least 5 μm apart from each other. The overall schematic of the resulting setup is presented in Figure 10.

Before indentation, the tip was brought into contact with the heated surface of the platinum and allowed to equilibrate for more than an hour at temperature. This allowed the system to

---

[6] For the derivation of this result from basic principles of Hertzian elastic theory, refer to Appendix B.
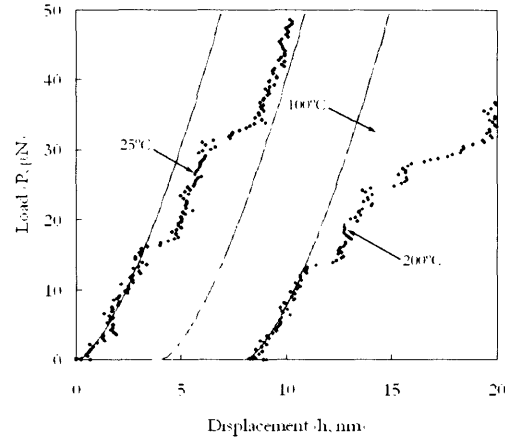
Figure 11: Representative load-displacement curves, performed at various temperatures. Note the absence of thermally induced noise. Curves for 100°C and 200°C offset for clarity.

thermally stabilize before the onset of indentation, and reduced thermal noise and drift to negligible levels, as is illustrated in Figure 11. Indentations for a given set of conditions were performed for the most part in a continuous period. The indenter tip remained continuously in physical and thermal contact with the surface during this time, under a constant applied load of 2 μN. The temperature indicated by the thermocouple on the sample therefore provided an accurate indication of the temperature of the platinum in the sampled volume.

The equilibrated temperature of the system during nanoindentation was varied between 25°C, 100°C, and 200°C. As the mechanical properties of diamond and platinum do not change appreciably in this range, the elastic portion of loading was approximated using the same reduced modulus E_R and the same indenter tip radius R as for room temperature. For every set of conditions, E_R was taken to be 172 GPa, as calculated from Equation (B.3) using the Poisson's ratios of 0.07 and 0.387 and the Young's moduli of 1140 GPa and 172 GPa for the diamond tip and the platinum sample, respectively [57]. The epoxy remained stable up to temperatures around 260°C, well beyond the range probed during the experiment.

The ability of the Hysitron Triboindenter to maintain continuous contact with the surface using the indenter tip, even while imaging or changing areas on the sample, prevented the onset of any plastic events related to elevated indenter momentum on contact [34, 39]. Furthermore, the diamond indenter tip did not interact strongly with the clean platinum surface, thereby avoiding
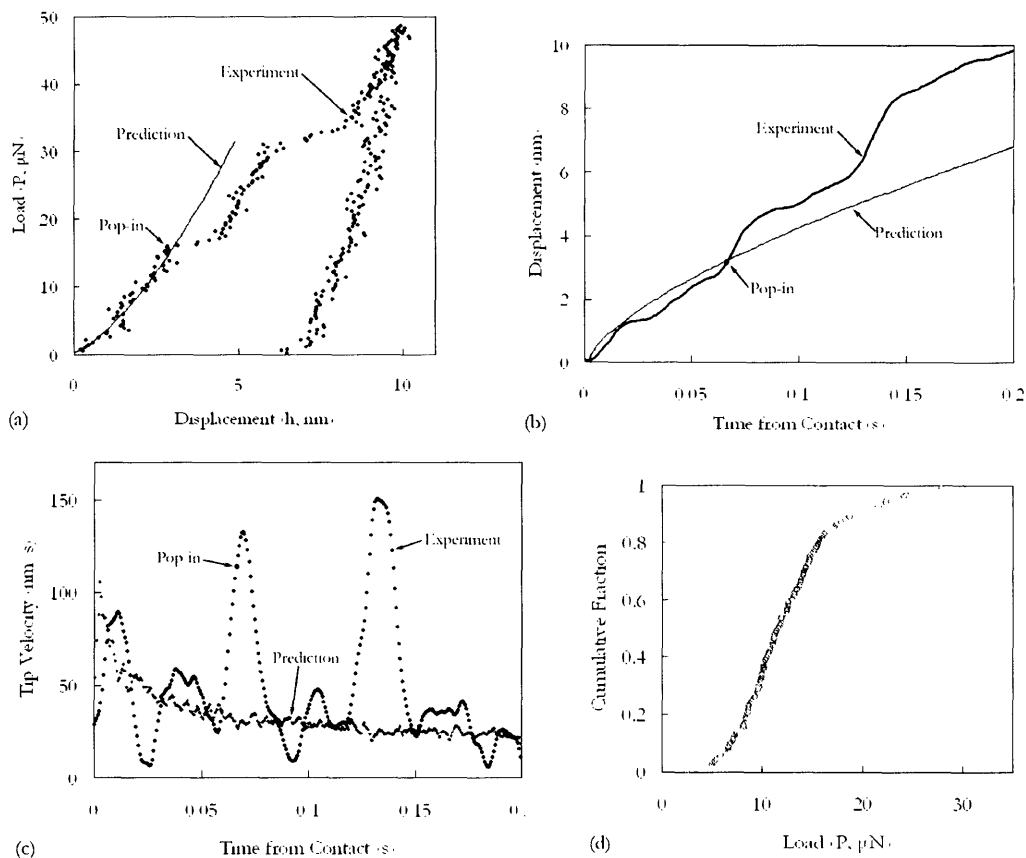
Figure 12: Example of a pop-in for an indent into (110) oriented single-crystal platinum at 25°C with a constant loading rate of 250 μN s⁻¹. Experiment gives values recorded from experiment, Prediction gives Hertzian elastic model for recorded loads, and Pop-in is determined to be the onset of plasticity. (a) Load-displacement curve of the indent. (b) Displacement of the indenter tip versus time. (c) Velocity of the indenter tip versus time. (d) Cumulative fraction of pop-ins versus load, for 158 indents.

jump-to-contact behavior occasionally observed during indenter tip approach. Further information regarding the Hysitron Triboindenter is available by request from Hysitron Inc.

2.2.3 IDENTIFICATION OF THE ONSET OF PLASTICITY

A variety of system variables allowed nanoindentation of platinum to be performed under a considerable range of conditions. Since the dislocation nucleation mechanism is expected to be a stochastic, thermally activated process, this study focused on the effects of variation in the

40

temperature and the loading rate. Raising the temperature of this type of process should reduce the necessary mechanical bias, and promote nucleation under smaller loads. Meanwhile, increasing the loading rate should allow less time for a favorable thermal fluctuation and permit higher loads to be achieved before the onset of plasticity. The majority of the indentations were therefore performed in (110) platinum at 25°C, 100°C, and 200°C, and at constant loading rates of 25 μN s^{-1}, 250 μN s^{-1}, and 2500 μN s^{-1}; more than 150 indentations were taken at each of the nine combinations of these loading rates and temperatures, for a total of 1398 indentations. This provided a baseline for the statistics governing the nucleation process. Indentations were then performed under several other sets of conditions, but without as substantial a statistical sampling as the ones specified above. Overall, 3062 indentations were recorded and evaluated during the duration of the experiment.[7]

For each indent, the Hysitron Triboindenter returned the data for several hundred points on the load-displacement curve, including values for the displacement of the indenter into the surface, the force applied to the indenter tip, and the time since the initiation of the loading function. An example of one of these curves appears in Figure 12(a). Identification of the pop-in, or the onset of plastic behavior, followed a straightforward procedure. The experimental values for the displacement versus time were initially passed through a double-low pass filter, to reduce the machine noise relative to the low-frequency behavior. A depiction of the result is shown Figure 12(b), along with the elastic Hertzian prediction for displacement versus time, derived from the recorded load values. The velocity of the indenter tip and the predicted velocity based on the Hertzian theory were then calculated at each point by taking the derivative of these curves, and are given in Figure 12(c). A pop-in is identified as the earliest point on the velocity-time curve where the actual indenter velocity exceeds the predicted velocity by a constant factor, in this case four. As indicated on Figure 12(a), the point identified on the velocity-time curve accurately captures the onset of deviation from Hertzian elastic behavior.

This pop-in identification procedure was performed for each of the indentations taken, and each one was verified by inspection of the load-displacement curve to ensure the accuracy of the algorithm. The tabulated results for one particular condition, in this case indentation into (110) oriented platinum at 25°C and at a constant loading rate of 250 μN s^{-1}, appear in Figure 12(d). The

---

[7] Each of these indentations appears in graphical format as a component of the appropriate cumulative fraction function in Appendix E.

choice was purposeful to display these results in terms of a cumulative fraction $F_E(P)$, or the fraction of the total number of indentations performed for which pop-in occurred at or before a particular applied load, instead of a frequency distribution. A frequency distribution must involve binning in order to display the results of a series of measurements; this process reduces the recorded accuracy of the load at which events occur. None of this information is neglected in a cumulative fraction graph.

2.3   MATHEMATICAL METHODS

This section outlines many of the mathematical equations and thoughts used to perform an analysis of the indentations. The necessary mathematics may be divided into three distinct subjects. A generic method must be outlined for turning the involvement of a physical event in the onset of plasticity into a mathematical model to be used for predictive purposes. A quantity must be defined to measure the accuracy of the resulting predictions, in order to distinguish one particular proposed model of incipient plasticity from other possibilities. A procedure must then be formulated for using this quantity to rapidly find the most accurate of the permissible models.

2.3.1   MODELING

Although nanoindentation is useful to observe the details of the onset of plastic deformation, an understanding of the relevant process is developed only through a predictive model. The above discussion implies a stress-biased, thermally-activated mechanism. Different theories attribute the initial plasticity to events occurring in different regions; that is, either at the surface, or within the volume of the crystal. Assume for the moment that the dislocation nucleation event occurs within the volume of the sample. Any given model for dislocation nucleation yields a mathematical function $\dot{n}(\sigma, T)$ describing the probability of a nucleation event in a unit volume in a unit time, where σ is the uniform stress state of the volume and T is the temperature of the volume. As a result of the convoluted nature of the stress fields underneath the indenter, the actual values of σ and of $\dot{n}(\sigma, T)$ depend strongly on position. For that reason, evaluation of this function in the

solid requires the components of the complete stress tensor to be calculated for every set of position coordinates and value of the applied load[8]. Integration over the stressed volume underneath the indenter then removes the dependence of the value of $\dot{n}(\sigma,T)$ on position, and is mathematically expressible as

$$\dot{N}(P,T) = \iiint_{\Omega} \dot{n}(\sigma,T)d\Omega.$$

(2.2)

This function $\dot{N}(P,T)$ is the probability of a dislocation nucleating in a volume in a unit time, where the stress state of the volume is identical to that of a solid beneath an indenter tip exerting a load of P on the surface[9]. Although the integral should theoretically extend throughout the entire crystal, only a restricted volume practically needs to be included; a nucleation event must physically happen in the vicinity of the indentation to participate in a displacement burst. Consequently, the integral is performed over a cylindrical volume extending into the sample from the surface, with a height equal to four times the contact radius, and a radius equal to three times the contact radius, as given by Equation (C.1)[10]. The volume integral, in cylindrical coordinates, then becomes

$$\dot{N}(P,T) = \int_{0}^{2\pi}\int_{0}^{4a}\int_{0}^{3a} \dot{n}(\sigma,T)r\,dr\,dz\,d\theta.$$

(2.3)

The shear stress and pressure on the boundary of this surface reach only about one-tenth the maximum values contained within the volume of the cylinder; nucleation occurring at stresses smaller than these outside of the included volume is unlikely. Since the contact radius is proportional to the extent of the stress field, the cylinder scales with the extent of the stressed volume, and maintains the set boundary condition for every external load. Extension of the integral to more expansive regions did not appreciably change the values of $\dot{N}(P,T)$, and therefore this volume is physically and mathematically reasonable.

---

[8] Equations involved in this calculation, as well as the process used to derive the quantities of local pressure and local shear stress, appear in Appendix C.

[9] The dependence of the probabilistic rate of nucleation on P derives from the dependence of σ on P, but this explicit dependence is suppressed in the interests of clarity.

[10] The dependence of the probabilistic rate of nucleation on P, using these limits of integration, further derives from the dependence of the contact radius on P, but this explicit dependence is suppressed in the interest of clarity.
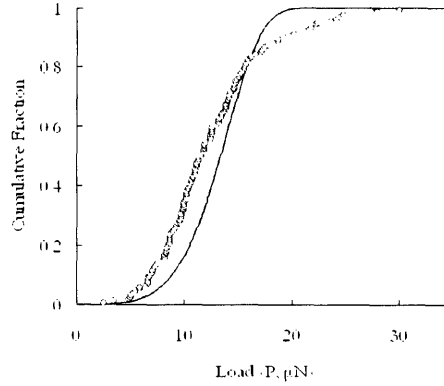
Figure 13: Example of experimental and predicted cumulative fraction functions for indents into (110) oriented single-crystal platinum at 25°C with a constant loading rate of 250 μN s[1]. Experimental curve appears in blue, and predicted curve appears in green.

Once the probabilistic rate of nucleation is determined, the predicted cumulative fraction of nanoindentation tests displaying plastic behavior as a function of time may be calculated[11]. This involves manipulating the integral of the nucleation rate over time, as

$$F_P(t,T) = 1 - \exp\left(\int_0^t \dot{N}(P,T)dt'\right) \qquad (2.4)$$

where $F_P(t,T)$ is the function describing the probabilistic prediction for the cumulative fraction of events in terms of the time t since initiation of the indentation[12]. Notice that while the temperature of the system enters explicitly into the cumulative fraction function, the loading rate and the form of the loading function enter only through the time integral. In this manner, predicted cumulative fraction functions may be found for each set of indentation conditions, based on the mathematical form of the proposed subsurface mechanism. A representative probabilistic prediction calculated using this procedure appears with the relevant experimental cumulative fraction curve in Figure 13.

A similar analysis may be conducted assuming that dislocation nucleation occurs in the only other available region; namely, the surface. The development of this kind of model provides the opportunity to compare conflicting ideas about the location of the initial event. A surface

---

[11] For a discussion of the calculation of cumulative fractions from probabilistic rates, refer to Appendix D.

[12] The dependence of the cumulative fraction function on t derives from the dependence of P on t through the specifications of the loading function, but this explicit dependence is suppressed in the interests of clarity.

44

mechanism requires a function $\dot{n}(\sigma, T)$ describing the probability of a dislocation nucleating in a unit area in a unit time, where σ is the uniform stress state of the area and T is the temperature of the area. Analogous to the volume based mechanism, the evaluation of the local stress state σ and the function $\dot{n}(\sigma, T)$ require the calculation of the complete stress tensor for every set of surface position coordinates and value of the applied load, due to the strong dependence of these functions on position[13]. The positional dependence of the nucleation rate is then removed by an integration over the stressed surface area, given by

$$\dot{N}(P, T) = \iint_A \dot{n}(\sigma, T) dA.$$
(2.5)

As before, this function $\dot{N}(P, T)$ is the probability of a dislocation nucleating in an area in a unit time, where the stress state of the area is identical to that of the surface area beneath an indenter tip exerting a load of P on the surface[14]. Considering that a nucleation event related to the displacement burst must happen in the vicinity of the indentation site, the integral is performed over a circular area of the surface centered on the initial point of contact with a radius equal to three times the contact radius, as given by Equation (C.1) [15]. This yields the function

$$\dot{N}(P, T) = \int_0^{2\pi} \int_0^{3a} \dot{n}(\sigma, T) r dr d\theta.$$
(2.6)

The probabilistic rate of nucleation $\dot{N}(P, T)$ then provides a predicted cumulative fraction function $F_P(t, T)$ exactly as above.

2.3.2   FITNESS CRITERION

The predicted results, in the form of cumulative fraction curves, may be calculated from any given $\dot{n}(\sigma, T)$ following the above procedure. Notice that the substantial freedom in the form of

---

[13] Equations involved in this calculation, as well as the process used to derive the quantities of local pressure and local shear stress, appear in Appendix C.

[14] The dependence of the probabilistic rate of nucleation on P derives from the dependence of σ on P, but this explicit dependence is suppressed in the interests of clarity.

[15] The dependence of the probabilistic rate of nucleation on P, using these limits of integration, further derives from the dependence of the contact radius on P, but this explicit dependence is suppressed in the interest of clarity.

45

$\dot{n}(\sigma, T)$ allows predictions to be made for a variety of models. Direct comparison of predictions made for different models is difficult though, unless a quantity is defined that captures the accuracy of the description of the dislocation nucleation process provided by a particular mechanism. This quantity is measured by the degree to which the predicted cumulative fraction curves match the experimentally determined ones, and is expressed by a sum of squares of the differences between the curves.

Each set of indentation conditions is a component of a family; index the components of this family with the label i, and allow i to vary from one to n, where n is the number of sets of indentation conditions. Each indentation performed using the specifications of the ith set of conditions is a component of a further family; index the components of this family with the label j, and allow j to vary from one to m, where m is the number of indentations performed using the ith set of conditions[16]. For the ith set of indentation conditions there further exists a predicted cumulative fraction function, $F_P^i(P)$, derived from the proposed nucleation mechanism, and an experimental cumulative fraction function, $F_E^i(P_j)$, derived from the results of the indentation experiments[17]. Notice that while the predicted cumulative fraction function is a continuous function of P, the experimental cumulative fraction function is a discrete function of P_j, where P_j is the applied load at pop-in for the jth indentation in the ith set of conditions; this reflects the finite number of indentations performed during the experiment.

The degree to which the predicted function $F_P^i(P)$ matches the experimental function $F_E^i(P_j)$ is derived from a point-by-point comparison. For the jth indentation in the ith set of conditions, find the square of the difference between $F_P^i(P_j)$ and $F_E^i(P_j)$. Repeat this process for each of the j indentations in the ith set of conditions, and average the results;

$$D' = \frac{\sum_{j=1}^{m} \left(F_E^i(P_j) - F_P^i(P_j) \right)^2}{m}. \tag{2.7}$$

---

[16] Generally, m is dependent on the value of i; that is, the number of indentations performed is different for each set of conditions.

[17] The dependence of the cumulative fraction function on T was incorporated into the complete set of indenting conditions, indexed by i. The dependence of the function on t was converted to a dependence on P though use of the set-specific loading function.

This provides a single value D' that expresses the average square of the difference between the experimental results and the predicted results for any number of indentations performed using the ith set of conditions. Notice that each indentation is weighted equally in the average; purposeful selection of results that support a favored model is not permissible with this fitness criterion. The square of the difference is used, not only to remove the sign dependence of the difference, but to heavily weight outlying points or regions in the experimentally determined cumulative fraction function. Dividing by the number of indentations performed using the ith set of conditions, denoted by m, gives the average squared difference per indentation. This average, which does not depend explicitly on the magnitude of m for the ith set of conditions, permits the value D' to be directly compared for different models or sets of indentation conditions.

To find the overall fitness of a particular model, repeat this process for each of the n sets, and average these values over the total number of indentations considered; mathematically, this is expressed by

$$D = \frac{\sum_{i=1}^{n}\sum_{j=1}^{m}\left(F_E^i(P_j) - F_P^i(P_j)\right)^2}{\sum_{i=1}^{n} m}. \tag{2.8}$$

The quantity D expresses the average square of the difference between the experimental results and the predicted results for any number of indentations, but includes indentations from each of the n sets of indentation conditions. Each indentation is weighted equally in the average, irrespective of the set of conditions in which that indentation was performed; as above, purposeful selection of results that support a favored model is not permissible with this fitness criterion. Notice that sets of conditions where m is relatively small do not contribute as heavily to the average as the others though, as is appropriate considering that the experimental cumulative fraction function for these sets of conditions is less statistically robust. The square weights outlying points or regions in each of the n cumulative fraction functions heavily, as before. Given that D denotes an average value for the match between the predicted function and the experimental function, and is not explicitly dependent on the number of included indentations m or sets of conditions n, this value may be directly compared for different models to evaluate their relative fitness, even as the number of included indentations changes from one evaluation to the next. As the value of D decreases, the predicted model fits the experimental results better.

2.3.3 MINIMIZATION ALGORITHM

Although D provides a convenient measure of the fitness of the predicted cumulative fraction functions generated for a particular probabilistic nucleation function $\dot{n}$, the evaluation of D for many functions $\dot{n}$) is rather computationally intensive. An iterative algorithm developed with this issue in mind rapidly searches families of related functions for the one that provides the smallest value of D. Define a family of functions, each expressible as $\dot{n}$, as every function that shares a common functional form; for example, the family of exponential functions. Components of this family may be distinguished by the values of certain available parameters; for example, the value of a constant coefficient. Define a sequence s of the available parameters for a given family of functions. Arbitrarily pick initial values for each of the parameters, and systematically vary the values over a local region in the space spanned by the elements of s. Evaluate D for each examined sequence, and finding the locally optimal values. These then become the basis for the next variation, and the process is repeated until a stable, optimized value for each parameter is found. These stable values are the values of the parameters that pick out the element of the family of functions $\dot{n}$ that best fit the predicted curves with the experimental ones.[18]

---

[18] An example of the overall fit between the predicted and experimental cumulative fraction functions that results from this procedure appears in Appendix E.

CHAPTER 3

RESULTS AND DISCUSSION

3.1 NUCLATION MODELS

From observations of the dependence of the pop-in effect on temperature [36], the probabilistic dislocation nucleation rate may reasonably be expected to follow a relation analogous to the Arrhenius Rate Law for chemical reactions, meaning that the rate of dislocation nucleation increases exponentially with the absolute temperature. Keeping this in mind, the research of Bahr *et al.* [33] and Schuh *et al.* [5, 36] suggest that the dislocation nucleation rate function follows the general form

$$\dot{n} = \eta_0 \exp\left(-\frac{\varepsilon - \sigma v}{kT}\right) \qquad (3.1)$$

where ε-σv is the activation energy for the reaction, kT is the average available thermal energy, and η_0 is the pre-exponential frequency factor. For the process under consideration, the activation energy is separated into a term characterizing the activation enthalpy of dislocation nucleation, represented by ε, and a term capturing the stress-bias of dislocation nucleation, represented by σv, where σ is a generic stress state acting over the activation volume v[19]. The stress-biasing term is included to account for the increased rate of dislocation nucleation at elevated stresses, and effectively reduces the activation energy for the nucleation process. This separation of the activation energy into individual components is made more transparent by expressing the function in the form

$$\dot{n} = \eta_0 \exp\left(-\frac{\varepsilon}{kT}\right) \exp\left(\frac{\sigma v}{kT}\right) \qquad (3.2)$$

where the first exponential term gives the probability per attempt of a dislocation nucleation event in a stress-free crystal, and the second makes explicit the exponential dependence of the rate of dislocation nucleation on applied stress. The pre-exponential frequency factor η_0 indicates the

---

[19] Refer to Appendix C for calculations of the relevant components of the complete stress tensor.

effective physical number of attempts at dislocation nucleation per second per unit volume of material[20]. Notice that the values for η_0, ε, and v reflect only the rate-limiting step in the dislocation nucleation process. Since the purpose of this study is to determine the nature of the dislocation nucleation event, η_0, ε, and v will be treated as fitting parameters in the optimization process. As the values of these noticeably depend on the specifics of the probabilistic dislocation nucleation rate function, the form of the model will be varied as well.

3.1.1 SHEAR-BIASED MODEL

The most straightforward nucleation function follows the assumption prevalent in the experimental literature that the dislocation nucleation process is shear controlled. Notice that this does not presuppose the action of a particular physical mechanism for nucleation, but merely that the process is shear-biased. The equation for this replaces the general stress state σ with a τ, representing the maximum shear stress sustained in the material and yielding

$$\dot{n}(\tau, T) = \eta_0 \exp\left(-\frac{\varepsilon}{kT}\right) \exp\left(\frac{\tau v}{kT}\right). \tag{3.3}$$

The procedure outlined in the Methods section is used to find optimal values of η_0, ε, and v for this nucleation function for any given family of indentation conditions. Three families present themselves as intuitively reasonable; the family of every indentation performed on the (110) surface, the family of every indentation performed on the (111) surface, and the combined results from the (110) and the (111) surfaces. These choices arise naturally from the physically distinct nature of the surface orientation, and allow quantification of the degree to which sampling on the (111) surface is not as statistically robust as on the (110) surface. Furthermore, this provides a convenient means to test the assumption that the activation mechanism is independent of sample orientation, as is implicit in the model proposed above. The evaluation of the nucleation function did not include indents on the (100) surface, due to insufficient sampling.

The results of the fitting procedure for each of these three families of indentation conditions appear numerically in Table 1. This includes the optimal values for each of the fitting parameters

---

[20] For simplicity in explanation, the nucleation mechanism will be assumed to be volume-based unless explicitly stated otherwise. Application of the concepts and techniques developed for a volume-based mechanism to a surface-based mechanism is performed by substituting unit areas for unit volumes.

Table 1: Optimal parameter values for the family of shear-biased,
exponential nucleation functions, as outlined in Equation (3.3).

Surface Orientation	(110)	(111)	Combined
Attempt Frequency ($s^{-1}m^{-3}$)	$1.78 \cdot 10^{26}$	$1.93 \cdot 10^{26}$	$3.61 \cdot 10^{25}$
Activation Enthalpy (eV)	0.276	0.374	0.305
Activation Volume ($Å^3$)	10.17	10.92	10.38
Fitting Criterion D	0.0076	0.0232	0.0171

η_0, ε, and v, as well as the value of D, to allow the fitted results to be compared. Notice how well the optimized values for the fitting parameters, especially the activation volume, correspond among the three families of indentations considered. This implies that elastic anisotropy and the variation in behavior based on available slip planes constitute relatively small effects, and may be overlooked for the purposes of developing an initial predictive model. Graphical representations of the cumulative fraction curves for the combined family of indentations appear in Appendix E. These predicted curves follow the experimental curves well enough that this simple shear-biased model serves as a baseline for comparison of other proposed models.

3.1.2 REVERSIBLE SHEAR-BIASED MODEL

As is readily apparent from observations of chemical reactions, thermodynamic considerations stipulate that many processes are to some extent reversible. That is, the energy barriers to reaction may be traversed in either direction. For the current situation, this suggests that there exists a finite probability of an already nucleated dislocation loop self-annihilating and leaving behind a perfect crystal[21]. The probability of a collapse is likely controlled by a rate-limiting step similar to the one for dislocation nucleation. This implies that the activation enthalpy, activation volume, and the attempt frequency for collapse are of nearly the same magnitude as for nucleation, and may be reasonably approximated as being equal. Applying the principle of reaction reversibility to the shear-biased model proposed above, the expression for the overall rate of dislocation nucleation in the sample is given by

---

[21] Mathematically, this model only incorporates the possibility of a reverse reaction for a shear-biased process, and does not presuppose the action of a particular mechanism. Discussion of the annihilation of a dislocation loop is meant only to illustrate an example of a reverse reaction.

Table 2: Optimal parameter values for the family of shear-biased, hyperbolic sine nucleation functions, as outlined in Equation (3.5).

Surface Orientation	(110)	(111)	Combined
Attempt Frequency (s^{-1}m^{-3})	$4.88 \cdot 10^{25}$	$3.98 \cdot 10^{26}$	$9.58 \cdot 10^{25}$
Activation Enthalpy (eV)	0.277	0.360	0.306
Activation Volume (Å^3)	9.84	10.17	10.07
Fitting Criterion D	0.0073	0.0226	0.0167

$$\dot{n}(\tau,T) = \eta_0' \exp\left(-\frac{\varepsilon}{kT}\right)\exp\left(\frac{\tau v}{kT}\right) - \eta_0' \exp\left(-\frac{\varepsilon}{kT}\right)\exp\left(-\frac{\tau v}{kT}\right) \tag{3.4}$$

where the first term represents the rate of dislocation nucleation, and the second term represents the rate of dislocation annihilation[22]. Notice that although each of these reactions must overcome the same enthalpy barrier, the local shear stress simultaneously encourages nucleation and discourages collapse, as is reflected in the equation by the change of the sign of the exponent in the shear bias exponential. Observing the similarity of the exponentials in Equation (3.4) to hyperbolic functions, the nucleation rate is recast into a simpler form, as

$$\dot{n}(\tau,T) = \eta_0 \exp\left(-\frac{\varepsilon}{kT}\right)\sinh\left(\frac{\tau v}{kT}\right) \tag{3.5}$$

where the pre-exponential factor η_0 absorbs the difference of a multiplicative constant[23]. This is identical to the shear-biased exponential model proposed above, except for a hyperbolic sine dependence on the stress-bias instead of an exponential dependence. This change in the functional form of the stress-dependence therefore reflects the consideration of a reverse reaction.

Optimization of the reversible shear-biased model used the same families of indentations as the simple shear-biased model in order to allow direct comparison of the models; every other proposed model used the same families of indentations as well, for this reason. The fitted results appear in Table 2. Apart from the same orientation independence, the most striking feature of the optimized parameter values is that they are the same as the ones for the simple shear-biased model, to within a few percent. Although D is slightly smaller for the reversible shear-biased model, the

---

[22] Although a collapse may only occur once a nucleation event has taken place, this restriction is not reflected in Equation (3.4). This expression is meant only as a mathematical representation of a first-order approximation for a reversible process.

[23] The extreme sensitivity of η_0 on the value of the parameters in either of the exponential terms renders only order-of-magnitude measurements of η_0 meaningful [55]. A constant factor of 2 may be reasonably neglected.

Table 3: Optimal parameter values for the family of pressure-biased, hyperbolic sine nucleation functions, as outlined in Equation (3.6).

Surface Orientation	(110)	(111)	Combined
Attempt Frequency ($s^{-1}m^{-3}$)	$1.92 \cdot 10^{26}$	$1.25 \cdot 10^{27}$	$3.70 \cdot 10^{26}$
Activation Enthalpy (eV)	0.273	0.338	0.297
Activation Volume (Å^3)	3.63	3.53	3.66
Fitting Criterion D	0.0080	0.0237	0.0173

difference is not statistically significant. The invariance of the optimized parameters with respect to the incorporation of a term for the reverse process suggests that the relevant event is nearly irreversible, and renders the integration of an annihilation term unnecessary.

3.1.3 REVERSIBLE PRESSURE-BIASED MODEL

Despite the utility of the body of mechanisms proposed in the literature for the development of mathematical models, the search for an accurate dislocation nucleation function must include models without extensive current theoretical justification, since the relevant event could be a physical process not yet considered. Conventional observation of bulk deformation of materials states that shear stress is responsible for plastic deformation. Nevertheless, in these sharply constrained volumes a radically different mode of dislocation nucleation may be activated, one that depends on the magnitude of the local pressure rather than the shear stress. This does not presuppose the action of a particular mechanism, but merely that the pressure gives the stress-bias. A model similar to the reversible shear-biased model outlined above, except with the general stress state σ replaced by the local mean pressure rather than the maximum shear stress, is considered to account for this possibility. The resulting dislocation nucleation rate function appears as

$$\dot{n}(\tau,T) = \eta_0 \exp\left(-\frac{\varepsilon}{kT}\right)\sinh\left(\frac{\sigma_p v}{kT}\right) \tag{3.6}$$

where σ_p is the local mean pressure. The numerical results of the optimization of this model are presented in Table 3.

Examination of the optimized parameters reveals that although η_0 and ε closely match the values for the simple shear-biased model, the values of v differ by a factor of about three. The

difference in the values of the activation volume may be attributed to the specifics of the mean pressure function and maximum shear stress function underneath the indenter though, rather than to the description of a fundamentally different mechanism. Recall that optimization is performed over the same families of indentations for the simple shear-biased model and for the reversible pressure-biased model. Given the resemblance of mathematical form and the similarity of values for η_0 and ϵ, the models are expected to yield comparable fits to the experimental results when the only other available components, the stress-biasing expressions τv and $\sigma_p v$, nearly equal each other. Although the stress values included in these terms vary considerably with position, the relative magnitude of pressure to shear stress is reasonably estimated by forming the ratio of their maximum values. This ratio, or the factor by which the pressure σ_p underneath the indenter exceeds the shear stress τ, is about 4.12, and is independent of the applied load. Equating τv and $\sigma_p v$ therefore entails setting the activation volume for the pressure-biased model three or four times smaller than the activation volume for the shear-biased model, exactly as is observed.

Meanwhile, the similarities in the activation enthalpy and attempt frequency reflect the same experimentally observed dependencies on temperature and loading rate. Most of the temperature dependence is captured in the exponential containing the activation enthalpy term, even though the exponential carrying the stress-bias depends on temperature as well. This happens because the stress-bias term is in general small compared to the activation enthalpy over the range in stresses where pop-in is observed. Since the experimental temperature dependence does not change for different models, stability of the activation enthalpy with respect to the form of the stress-bias is reasonable. As for the attempt frequency, η_0 is closely related to the time dependence of dislocation nucleation, which enters through variations in the loading rates. Reductions in the loading rate allow more time for a favorable thermal fluctuation to occur earlier in the loading function, and encourage dislocation nucleation at smaller loads. The magnitude of this effect is directly related to the number of attempts per second, or η_0. Since the dependence of the pop-in statistics with variation in the loading rate does not change for different models, stability in the attempt frequency with respect to the form of the stress-bias is expected as well.

The use of pressure in the dislocation nucleation function does not provide any additional understanding of the stress-bias, temperature dependence, or loading rate dependence of the dislocation nucleation process. Furthermore, the fit is not appreciably more accurate than for the simple shear-biased model, as measured by the respective values of D. Nevertheless, these models

Table 4: Optimal parameter values for the family of shear-biased, exponential nucleation functions reflecting pressure-induced hardening, as outlined in Equation (3.7).

Surface Orientation	(110)	(111)	Combined
Attempt Frequency (s^{-1}m^{-3})	$2.02 \cdot 10^{25}$	-	$4.76 \cdot 10^{25}$
Activation Enthalpy (eV)	0.286	-	0.318
Activation Volume (Å^3)	18.85	-	19.85
Fitting Criterion D	0.0073	-	0.0168

may be compared on the basis of the physical implications of their parameter values. Observe that the volume of an atomic site in the lattice, given by the cube of the Burgers vector, is approximately 21.55 Å^3. The pressure-biased model therefore predicts that the pressure acts over an unreasonably small, sub-atomic region during the nucleation of a dislocation, and is consequently removed from further consideration.

3.1.4   SHEAR HARDENING MODEL

The pressure could enter into the dislocation nucleation function in some other manner; for example, the activation enthalpy may include a pressure dependent term. Certain materials exhibit elevated strength as pressure increases. This effect is believed to be related to a pressure induced change in the activation enthalpy for dislocation motion [58]. Perhaps the observed change in activation enthalpy for dislocation motion is indicative of a more general dependence of the energy of a dislocation on pressure. Since dislocation nucleation by definition generates dislocations, the activation enthalpy for dislocation nucleation could conceivably be pressure dependent as well. The dislocation nucleation rate function incorporates this modification to the simple shear-biased model as

$$\dot{n}(\tau,T) = \eta_0 \exp\left(-\frac{(1+\alpha\sigma_p)\varepsilon}{kT}\right)\exp\left(\frac{\tau v}{kT}\right) \tag{3.7}$$

where the magnitude of the effect is measured by the multiplicative factor α. From the evaluation of calculations performed in the literature [58], the value of α is estimated as 0.17 GPa^{-1} for platinum. The results of the fitting procedure for this model appear in Table 4.

The orientation independence of the statistics of dislocation nucleation is by this point readily evident from the similarity of the optimal fitting parameters for the different families of indentations used. For the shear hardening model, the completion of the fitting procedure for the (110) and combined families of indentations rendered the evaluation of the (111) family superfluous. With respect to the parameter values as determined by the fitting procedure, notice the relative elevation of the activation volume compared to the other proposed models. This is justifiable on the basis that pressure-induced hardening effectively increases the activation enthalpy, and the magnitude of the stress-biasing term must accordingly increase to overcome the enthalpy barrier and nucleate dislocations. As a result, the inclusion of the pressure-induced hardening effect expands the activation volume into the range of an identifiable structure in the crystal, namely a single occupied lattice site. Although this model is in this sense more physically reasonable than the others already considered, the meaning of a shear-bias within the confines of the proposed mechanism is unclear. Pressure-induced hardening assumes that the rate-limiting step is related to the presence or the nucleation of a dislocation of sufficient length to be described in continuum mechanical terms. The activation volume implicates the interaction of a single atom with the dislocation in order to bring about unstable dislocation expansion. Apart from these structures existing on distinctly different scales, making the dependence of the dislocation behavior on the motion of a single atom unlikely, the theoretical justification of the manner in which a shear stress biases the behavior of a single atom is vague. The relative probability of the presence of a pressure-induced hardening effect is therefore uncertain on the basis of these considerations alone.

3.1.5 VACANCY MIGRATION MODEL

Several studies in the literature theorize that the onset of plasticity could be related to the climb of a dislocation loop by vacancy absorption until a critical radius for unstable expansion is reached [14, 15, 56]. The rate limiting event for this process appears to be vacancy migration, and a model is formulated to investigate this type of mechanism. Recall that the energy of a vacancy is strongly dependent on pressure. A pressure gradient creates a corresponding energy gradient, and a driving

force for vacancy migration[24]. Although the pressure gradient is a vector, the directional component is unnecessary to determine the probability of a migration event; as a result, the magnitude of the gradient $|\nabla\sigma_P|$ is the relevant quantity. Furthermore, the pressure gradient has units of a pressure per length, and must be evaluated over a length distance. The pertinent length for vacancy migration in a solid is the inter-atomic spacing, and is equal to the Burgers vector b for the material. These considerations yield a stress-bias to the activation energy of $|\nabla\sigma_P|v_f b$, where v_f is the vacancy volume.

One more aspect inherent to vacancy migration should be considered. Vacancy migration requires that the crystalline lattice in the region of the vacancy be activated, or forced open to generate a free volume in excess of the vacancy volume before migration will occur. This excess volume is used to encourage the motion of the vacancy, is limited in extent by nearby occupied lattice sites, and is represented by the quantity v_m. Since vacancy activation involves a volume change, the relevant stress used to evaluate the energy requirement is pressure instead of the pressure gradient. Within the framework of a dislocation nucleation rate function, this appears as $\sigma_P v_m$. Consideration of the energy of the complete event then yields

$$\dot{n} = \chi_0 \exp\left(-\frac{\varepsilon_m + \sigma_P v_m - |\nabla\sigma_P|v_f b}{kT}\right). \tag{3.8}$$

The pre-exponential factor χ_0 represents the number of attempts at dislocation nucleation per second per unit volume, accounting for the concentration of vacancies in the sample. ε_m is the enthalpy of vacancy migration, and is expected to be in the range of 1.4 eV as reported in the literature [4].

Experiments on the effects of pressure on vacancy migration indicate that the excess volume v_m is directly proportional to the vacancy volume v_f [59]. For this model, the constant of proportionality α is used as a fitting parameter. The dislocation nucleation rate may then be presented as

$$\dot{n} = \chi_0 \exp\left(-\frac{\varepsilon_m}{kT}\right)\exp\left(\frac{(|\nabla\sigma_P|b - \alpha\sigma_P)v}{kT}\right). \tag{3.9}$$

---

[24] Pressure and the pressure gradient do not follow the continuum mechanical predictions when evaluated on atomic scales. Nevertheless, the continuum mechanical prediction is expected to give a reasonable approximation.

Table 5: Optimal parameter values for the family of vacancy migration functions, as outlined in Equation (3.9). Alpha is initially set to 0.0; increasing alpha increases the value of D. Activation volume is reported as the minimum value permitted by the fitting procedure.

Surface Orientation	(110)	(111)	Combined
Attempt Frequency (s^{-1}m^{-3})	2.49 ·10^{24}	1.95 ·10^{25}	4.75 ·10^{24}
Activation Enthalpy (eV)	0.109	0.177	0.131
Activation Volume (Å^3)	0.02	0.02	0.02
Fitting Criterion D	0.070	0.0688	0.0730

The results of the fitting procedure for this model appear in Table 5. Observe that the value of D for each of the families evaluated is much higher than the value of D for any of the other models. This indicates that accurate predicted cumulative fraction functions could not be found for any values of the available parameters within the confines of this model. Further shortcomings include an optimized value of activation enthalpy only one-tenth as large as 1.4 eV, and optimized values of the activation volumes smaller than the minimum value permitted by the current implementation of the fitting algorithm. The vacancy migration model is clearly unphysical, and is excluded from further consideration.

The failure of the vacancy migration model seems to be related to a curious feature of the pressure distribution predicted by Hertzian contact mechanics; the pressure gradient evaluated over a differential element of volume remains constant, provided that the spatial coordinates of the differential element scale with the contact radius, and the differential volume scales with the cube of the contact radius. This apparently results from the self-similar nature of the pressure field. The value of the stress-bias expression is therefore nearly a constant, rendering the model unable to accurately capture the increase in nucleation rate with applied load.

3.1.6 VACANCY DISSOCIATION MODEL

Perhaps a vacancy is involved in dislocation nucleation, but through a mechanism much different from migration. Allow shear stress to remain the bias for the rate-limiting event. Shear stresses in general encourage a sliding of one part of the crystal relative to an adjacent part, or a relative
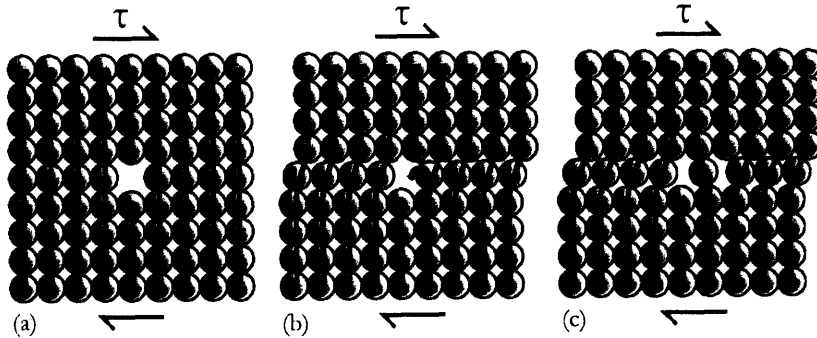
Figure 14: Proposed vacancy dissociation mechanism. (a) Crystal containing a vacancy under a shear stress. (b) Distortion of the crystal and vacancy by the shear stress. (c) Dissociation of vacancy into partial vacancies and edge dislocations.

displacement of adjacent atomic planes. Although the deformation response to shear stress in a perfect crystal would remain completely elastic for small stresses, a vacancy could provide a weak point in the lattice. That is, a shear stress in the region of a vacancy could initiate plastic deformation before the onset of homogenous dislocation nucleation, through a mechanism of vacancy dissociation. This is reflected schematically in Figure 14.

Consideration of the atomic planes in the vicinity of a vacancy implies that the vacancy may be regarded as an effective dislocation loop, with a Burgers vector perpendicular to the plane of the dislocation. Examination of a single atomic plane containing the vacancy, as in Figure 14(a), reduces this to an edge dislocation dipole. Applying a shear stress to the configuration in Figure 14 encourages the effective upper dislocation to move to the right, and the lower effective dislocation to move to the left. The result is a division of the free volume of the vacancy, and the release of a pair of edge dislocations into the crystal at shear stresses less than the critical value for homogenous dislocation nucleation. Returning to the complete crystalline lattice, a vacancy dissociation event is analogous to the distortion of a dislocation loop in the direction of the shear stress. This dislocation nucleation mechanism is simply the limiting case of an event discussed at more depth in the literature [60].

Shear stresses may therefore act as the stress-bias in a dislocation nucleation model based on vacancy dissociation. As with the vacancy migration model, the dissociation of the vacancy probably requires the generation of a free volume v_m in excess of the vacancy volume v_f for the initiation of the relevant event. An energy given by $\sigma_p v_m$ must be expended to open this volume in the crystalline lattice. Mathematically, these considerations appear as

Table 6: Optimal parameter values for the family of shear-biased, exponential nucleation functions reflecting vacancy dissociation, as outlined in Equation (3.11).

Surface Orientation	(110)	(111)	Combined
Attempt Frequency (s^{-1}m^{-3})	$1.61 \cdot 10^{25}$	$1.49 \cdot 10^{26}$	$3.32 \cdot 10^{25}$
Activation Enthalpy (eV)	0.277	0.366	0.308
Activation Volume (Å^3)	14.52	15.22	14.94
Fitting Criterion D	0.0075	0.0230	0.0169

$$\dot{n}(\tau, T) = \eta_0 \exp\left(-\frac{\varepsilon + \sigma_p v_m - \tau v_f}{kT} \right) \tag{3.10}$$

where τv_f is the shear stress-bias. As before, v_m is directly proportional to the vacancy volume v_f, where the constant of proportionality is given by α. A value of 0.25 for α is considered reasonable for the noble metals [59]. The dislocation nucleation rate function is then

$$\dot{n}(\tau, T) = \eta_0 \exp\left(-\frac{\varepsilon}{kT} \right) \exp\left(\frac{(\tau - 0.25\sigma_p)v}{kT} \right) \tag{3.11}$$

with one exponential containing the activation enthalpy term and the other containing an effective stress-bias term. The parameter values from fitting this model to the experimental results appear in Table 6.

As may be expected from the similarities in mathematical form and the use of the same families of indentations, the optimal values of η_0, ε and D for the shear-biased vacancy model closely match those from the simple shear-biased model. The difference is primarily in the value of the activation volume; the vacancy dissociation model predicts activation volumes about one-and-a-half times higher than the simple shear-biased model. This is in some sense analogous to the analysis of pressure as the biasing stress. Note that every quantity is the same for the vacancy dissociation model as for the simple shear-biased model, except for the respective stress-bias expressions $(\tau - 0.25\sigma_p)v$ and τv. For that reason, the comparable fits to the experimental results for the models require that the magnitudes of $(\tau - 0.25\sigma_p)v$ and τv be nearly the same. The analysis used for the reversible pressure-biased model does not apply directly though; the reversible pressure-biased model only considered the magnitude of the pressure field, while in this case the spatial dependence of the fields within the solid must be accounted for as well. Since the regions of peak shear stress and pressure do not overlap, the effective reduction in the stress value by subtracting

the pressure field is less than would be otherwise expected. Nevertheless, $(\tau-0.25\sigma_p)$ is everywhere smaller than τ and the activation volume for the vacancy dissociation model is expected to be higher than that of the simple shear-biased model, as is observed.

Notice that even though the mechanism for the vacancy dissociation model is presupposed, and in that sense qualitatively different from the mechanism in the simple shear-biased model, the values for each of the fitting parameters remain remarkably similar. A direct comparison of the fitting parameters suggests that the vacancy dissociation model is the more physically plausible though. The accepted, unstressed value for v_f is 0.72 b^3 or 15.5 $Å^3$, and is substantially smaller than the volume of an occupied lattice site due to the relaxation of the lattice into the free volume [4]. The presence of a pressure further reduces the vacancy volume by

$$\Delta v = v \cdot \frac{P}{K} \tag{3.12}$$

where K is the bulk modulus of 276 GPa in platinum. Evaluated for realistic pressures underneath the indenter, this accounts for a change of a further few percent. The resulting value for the expected vacancy volume in indented platinum is remarkably close to the calculated vacancy dissociation model activation volume of 14.94 $Å^3$, and is much more physically reasonable than the 10.38 $Å^3$ predicted by the simple shear-biased model.

3.1.7 SURFACE MODEL

One of the variables discussed in the literature as pertinent to the onset of plastic deformation is the presence of asperities or ridges on the surface of the crystal [34, 39]. Mechanisms involving the presence of surface roughness, or any rate limiting event taking place on the surface of the sample, entail a different mathematical form and fitting procedure from the models considered above. Specifically, the relevant function must evaluate the probability of a dislocation nucleation per second per unit area rather than per unit volume. This requires altering the pre-exponential factor η_0 to represent the number of attempts at dislocation nucleation per second per unit area of the sample surface. Since the model must reflect the experimentally observed thermally-activated, stress-biased nature of the initial event, the form of the nucleation rate function for a surface

Table 7: Optimal parameter values for the family of shear-biased, exponential nucleation functions reflecting the action of a surface mechanism, as outlined in Equation (3.13).

Surface Orientation	(110)	(111)	Combined
Attempt Frequency (s⁻¹m⁻²)	$4.58 \cdot 10^{19}$	$3.60 \cdot 10^{20}$	$8.58 \cdot 10^{19}$
Activation Enthalpy (eV)	0.760	0.984	0.836
Activation Volume (Å³)	199.82	244.88	216.15
Fitting Criterion D	0.0081	0.0220	0.0183

mechanism is otherwise the same as for a mechanism active in the bulk. Assuming a shear-biased event, this gives an initial surface model of

$$\dot{n}(\tau, T) = \eta_0 \exp\left(-\frac{\varepsilon}{kT}\right) \exp\left(\frac{\tau v}{kT}\right). \tag{3.13}$$

The fitting procedure for the class of surface based mechanisms is outlined in the Methods section, and results in the optimized parameter values appear in Table 7.

Notice that from the D criterion that the surface model follows the trends in the indentation statistics nearly as well as many of the models above. The values of the activation enthalpy and activation volume are substantially higher though, and make explicit the explanation of the indentation statistics though a mechanism of fundamentally different character. Hence, the relative probability of a surface event is not directly determinable without further analysis of the implications of the parameter values.

3.2 MODEL EVALUATION

The current understanding of the onset of plasticity during nanoindentation derives primarily from simulations, and involves the homogenous nucleation of dislocations. Consider the values of the attempt frequency, activation enthalpy, and activation volume expected for homogenous dislocation nucleation[25]. From continuum mechanical expressions of the energy of a dislocation, the critical volume required to form a stable dislocation loop is expected to be in the range of ten

---

[25] For simplicity in explanation, the nucleation mechanism will be assumed throughout this section to be volume-based unless explicitly stated otherwise.

to hundreds of atomic volumes, depending on the specific conditions of indentation [14, 20, 33]. The motion of this volume of material certainly requires an activation enthalpy of several eV, and is expected to be much more than the energy for point defect migration in the solid. As for the attempt frequency, the physical counterpart to this mathematical quantity is the number of vibrations of available nucleation sites in the sample per second per unit volume [33]. The characteristic vibrational frequency for a crystalline solid is given by the Debye frequency, and is about $5 \cdot 10^{12}$ s^{-1} for platinum. The nature of homogenous nucleation implies that a preferred site does not exist within the sampled volume, and that each lattice point is considered as an available site for nucleation; the number density of occupied lattice points in platinum is about $6.6 \cdot 10^{28}$ m^{-3}. A mechanism of homogenous dislocation nucleation predicts an attempt frequency in the range of the product of these quantities, reduced by the number of atoms involved, or about 10^{40} $s^{-1}m^{-3}$.

Recall the ranges in predicted values for the activation volume, activation enthalpy, and attempt frequency obtained from fitting a number of models to a statistically significant sampling of indentations. The activation volume is almost invariably less than a single atomic volume, but this is supported experimentally for the current interpretation of the indentation statistics by similar values found in previous studies [5, 55]. Meanwhile, the activation enthalpy is only a fraction of an electron volt, and the attempt frequency is in the range of 10^{26} $s^{-1}m^{-3}$. These values appear to be remarkably stable, and remain nearly the same for the variety of models and presupposed mechanisms considered. Of the observed quantities, the difference in the value of the attempt frequency predicted for the case of homogenous dislocation nucleation and the value observed from experiment is the most significant, around a factor of 10^{15}. Only the characteristic vibrational frequency and the number of available nucleation sites per unit volume enter into the calculation of the attempt frequency. As a characteristic property of the material, the Debye frequency is unable to account for the observed discrepancy. The number of experimentally determined sites available for dislocation nucleation must therefore be smaller than the number of occupied lattice sites by a factor of 10^{15}. A sparse distribution of available dislocation nucleation sites is an inherent characteristic of a heterogeneous nucleation event. This analysis is consistent with the observed activation enthalpy and activation volume, as each of these differs substantially from the values expected for homogenous dislocation nucleation. The initiation of plasticity by a homogenous dislocation nucleation mechanism is consequently inconsistent with the results of experimental nanoindentation, despite the prevailing understanding.

63

This leaves open the question of what precisely occurs during the onset of plastic deformation. As part of an initial evaluation, characteristics of the active mechanism may be surmised from the above discussion. Certain observable dependencies of the indentation statistics on temperature and applied load imply that the mechanism is thermally-activated and stress-biased. Consideration of the attempt frequency suggests that the process is heterogeneous in nature, involving sparsely distributed nucleation sites. From reflection on the results of modeling, a nearly complete independence of the mechanism on sample orientation is revealed by the stability of the derived parameter values with respect to the family of indentations used. Since the incorporation of a term for a reverse event did not improve the quality of the fit to within the resolution of the fitting procedure, the relevant mechanism is practically irreversible. As for the nature of the stress-bias, the involvement of the pressure gradient is excluded on purely mathematical grounds, and the action of a pressure-bias reduces the activation volume to physically unreasonable, subatomic levels. Of the various stress quantities considered, shear stress is the most probable candidate.

Evaluating the proposed mechanisms with respect to these necessary features, only the simple shear-biased model, the shear hardening model, and the vacancy dissociation model remain as possible candidates. Differentiation of the remaining models at this point continues on more practical grounds. Begin with the simple shear-biased model. Although this model provides accurate predicted cumulative fraction curves, the resulting value for the activation volume is only 10.38 Å^3. This volume is less than half the volume of an occupied lattice site, and does not obviously correspond to the volume of any element of structure in a crystalline material; the simple shear-biased model is in some regard not physically justifiable. Next, consider the shear hardening model. The proposed effect incorporated into this model is questionable on theoretical grounds, particularly in light of the experimentally determined values of the fitting parameters. A process controlled by the motion of a single atom that involves the unstable expansion of a dislocation is difficult to imagine. Furthermore, the motion of the relevant atom, presumably by migration, is more likely to be a result of a pressure gradient than a shear stress; the involvement of a pressure gradient in the stress-bias is already excluded though on mathematical grounds. While the shear hardening model is therefore as able to predict the indentation statistics generated by exhaustive experimental sampling as either of the others under consideration, the explanation of the pop-in event offered by the shear hardening model is unsatisfying.

Neither inaccurate predictions nor unphysical values of the optimal parameters hamper the vacancy dissociation model. The vacancy dissociation model returned one of the smallest values of D from the full range of models considered, and provides some of the most accurate descriptions of the indentation statistics observed. With respect to the parameter values, the proposed mechanism predicts an activation volume on the order of a vacancy volume in platinum, as is observed to within a few percent. Given that a vacancy dissociation event is similar to a partial vacancy migration, the predicted activation enthalpy is expected to be somewhat smaller than 1.4 eV in platinum. Specifically, vacancy dissociation entails the relative displacement of one plane of atoms relative to an adjacent plane, rather than the displacement of a single atom to the entire surrounding crystal. By leaving the involved atom stationary with respect to many atomic neighbors, the vacancy dissociation event only requires the breakage of about a quarter as many bonds as the relocation of an atom during vacancy migration. Hence, vacancy dissociation predicts an activation enthalpy about one quarter of the vacancy migration energy of 1.4 eV, as is observed to within reasonable experimental uncertainty.

An understanding of the initiation of plastic deformation by heterogeneous nucleation of dislocations involving a vacancy dissociation mechanism therefore provides a theoretically substantive and experimentally verified predictive model for the onset of plasticity[26]. Of the proposed models, this is considered the most probable one for dislocation nucleation in the bulk; the surface model offers an ideological alternative. The activation volume for the surface model suggests a mechanism involving about ten atomic volumes on the surface of the crystal, and is physically probably a component of either an asperity or a surface step. A value of the activation enthalpy slightly less that one electron volt is rather small for the barrier limiting the motion of this volume, but could be justified by the weak bonding of atoms on the surface of the crystal compared to atoms in the bulk. As a result, the surface mechanism is internally consistent with the fitted parameter values, and is considered a reasonable possibility as well.

---

[26] This does not mean to imply that this is the only possible mechanism with these qualities, merely that this mechanism is in accordance with the observed indentation statistics and that this mechanism is the most likely of the ones considered.

3.3 CONCLUSIONS

Scientific endeavors and technological innovations depend critically on the control of material behaviors and properties on ever-decreasing scales. Nanoindentation allows the characteristics of materials to be studied conveniently on the nanometer level, although the current understanding of the specifics of the material response to this technique is incomplete; one example is the mechanism of incipient plasticity. Despite being fundamental to the nanomechanical deformation of materials, the nature of the onset of plasticity as marked by an initial displacement burst remains contested in the scientific literature. Through cutting-edge experimental techniques and novel methods of statistical analysis, this study examined the statistical dependencies of the initial displacement burst on an oxide-free surface in an effort to provide further insight into the mechanism underlying this event. Our results include several critical quantities characterizing the atomic level mechanisms of incipient plasticity, quantified here for the first time.

3.3.1 SUMMARY OF RESULTS

The most important results of the current effort have been:

1. Development and implementation of a high-temperature nanoindentation technique. This allowed for the collection of high-quality nanoindentation data at multiple temperatures, with nanometer and micronewton resolution.

2. Formulation of rigorous mathematical procedures to efficiently and reliably compare the statistical predictions of various mechanistic models to the experimental data.

3. Experimental confirmation that the initial displacement burst is a stochastic, thermally-activated and stress-biased process, as proposed on theoretical grounds in the literature.

4. The rate-limiting event for incipient plasticity was found to occur over a single atomic volume with an activation energy of a fraction of an electron volt; these values are inconsistent with the expectations of a homogenous dislocation nucleation mechanism, and point strongly to a heterogeneous nucleation event.

5. Development of novel mechanisms for the initiation of plasticity through heterogeneous dislocation nucleation, including a vacancy dissociation model.

3.3.2 FUTURE RESEARCH

The results of this study at once suggest several directions for future research. Most notably, since dislocations appear to nucleate heterogeneously underneath the indenter tip, simulations meant to sensibly investigate the events happening during experimental nanoindentation must be performed into samples of material containing realistic distributions of flaws and surface roughness. The results of these simulations would be more directly related to experimentally observed behaviors than for simulations of perfect crystals, which currently dominate the literature. With respect to experiment, nanoindentation is now able to reliably identify the active mechanism during the onset of plasticity, and contribute to the development of a predictive dislocation nucleation theory. By acquiring a statistically significant sampling of displacement burst behavior into a wide variety of materials, orientations, temperatures and loading conditions, models reflecting different mechanisms may be distinguished easily on the basis of their predictions, and assessed for their relative suitability. The vacancy dissociation mechanism outlined herein deserves further study as a well, and may be decisively evaluated based on indentations into samples that explicitly vary the vacancy fraction in the material.

APPENDIX A

EQUILIBRIUM VACANCY FRACTION

The equilibrium fraction of vacancies in a crystal with N occupied sites and n vacancies is found by minimizing the free energy of the system with respect to n. Allowing Δh_f to be the enthalpy of formation for a single vacancy, the total difference in enthalpy between a crystal in thermodynamic equilibrium and a perfect crystal is

$$\Delta H_f = n\Delta h_f.$$

(A.1)

Meanwhile, the change in entropy contains several terms. For each vacancy introduced into the crystal, there is a change in entropy given by Δs_v that is related to the increased freedom of the local vibrational modes, and a further change in entropy related to the mixing of occupied sites and vacancies. The total change in entropy from the ideal reference state is the sum of these contributions, or

$$\Delta S = n\Delta s_v + k \ln \frac{(N+n)!}{N!n!}$$

(A.2)

where $(N+n)N!/n!$ is the number of possible combinations of N occupied sites and n vacancies. Substituting these expressions into the equation for free energy to find the change compared to the ideal reference state yields

$$\Delta G = n(\Delta h_f - T\Delta s_v) - kT[(N+n)\ln(N+n) - N \ln N - n \ln n]$$

(A.3)

where Sterling's approximation was used to simplify the logarithm. Thermodynamic equilibrium corresponds to the minimum of this function, which is found by setting the first derivative with respect to n to 0, or

$$\frac{\partial \Delta G}{\partial n} = \Delta h_f - T\Delta s_v + kT \ln \frac{n}{n+N} = 0$$

(A.4)

Rearranging this result allows the equilibrium fraction of vacancies to be expressed as

$$x_v = \frac{n}{n+N} = \exp\left(\frac{\Delta s_v}{k}\right)\exp\left(-\frac{\Delta h_f}{kT}\right) \; [2].$$

(A.5)

APPENDIX B

INTRODUCTION TO HERTZIAN THEORY

Hertzian theory provides a variety of computational tools to analyze elastic deformation during nanoindentation. Assuming that plastic deformation begins once the shear stress reaches a critical value, the maximum shear stress τ_{max} sustained by the elastically deforming solid for a given set of loading conditions may be found by

$$\tau_{max} = 0.47 \cdot \frac{P}{\pi R h} \qquad (B.1)$$

where P is the applied load, R is the effective radius of the indenter, and h is the displacement of the indenter into the surface. Since the initial contact closely follows the Hertzian elastic prediction, the applied load is expressible in terms of the indenter displacement, given by

$$P = \frac{4}{3} \cdot E_R \cdot \sqrt{R h^3} \,. \qquad (B.2)$$

E_R is the reduced modulus of the indenter tip-sample system, calculated as

$$\frac{1}{E_R} = \left(\frac{1 - v^2}{E} \right)_I + \left(\frac{1 - v^2}{E} \right)_S \qquad (B.3)$$

where v is Poisson's ratio, E is the Young's modulus, and the subscripts I and S indicate the properties of the indenter and substrate, respectively [61]. Combining Equation (B.1) with a inverted version of Equation (B.2) gives an expression for the maximum shear stress in terms of only system properties and the applied load;

$$\tau_{max} = \frac{0.47}{\pi} \cdot \left(\frac{4 E_R}{3R} \right)^{2/3} \cdot P^{1/3} \,. \qquad (B.4)$$

APPENDIX C

CALCULATION OF THE FULL STRESS TENSOR

The calculation of the stress states underneath the indenter before the initiation of plasticity follows the Hertz solution for elastic contact of a sphere on a half-volume. Strictly speaking, the following equations for the stress states of the elastic medium only apply when the tip of the indenter may be approximated as a sphere with a radius much larger than the radius of the contact area. With this constraint in mind, the radius of the contact area, denoted by a, is given by

$$a = \left(\frac{3PR}{4E_R}\right)^{1/3}$$ (C.1)

where R is the radius of the indenting sphere, P is the applied load, and E_R is the reduced modulus of the indenter and the substrate as in Equation (B.3). The average applied load is found by dividing the total applied load by the contact area, or

$$p_m = \frac{P}{\pi a^2}.$$ (C.2)

Using cylindrical coordinates (r, θ, z), where z measures the depth into the half-volume from the surface and r measures the distance parallel to the surface from the point of initial contact, the nonzero components of the stress tensor are given by

$$\frac{\sigma_{rr}(r,z)}{p_m} = \frac{3}{2}\left\{\frac{1-2\nu}{3}\frac{a^2}{r^2}\left[1-\left(\frac{z}{u^{1/2}}\right)^3\right]+\left(\frac{z}{u^{1/2}}\right)^3\frac{a^2 u}{u^2+a^2 z^2}+\frac{z}{u^{1/2}}\left[u\frac{1-\nu}{a^2+u}+(1+\nu)\frac{u^{1/2}}{a}\tan^{-1}\left(\frac{a}{u^{1/2}}\right)-2\right]\right\}$$

$$\frac{\sigma_{\theta\theta}(r,z)}{p_m} = -\frac{3}{2}\left\{\frac{1-2\nu}{3}\frac{a^2}{r^2}\left[1-\left(\frac{z}{u^{1/2}}\right)^3\right]+\frac{z}{u^{1/2}}\left[2\nu+u\frac{1-\nu}{a^2+u}-(1+\nu)\frac{u^{1/2}}{a}\tan^{-1}\left(\frac{a}{u^{1/2}}\right)\right]\right\}$$ (C.3)

$$\frac{\sigma_{zz}(r,z)}{p_m} = -\frac{3}{2}\left(\frac{z}{u^{1/2}}\right)^3\left(\frac{a^2 u}{u^2+a^2 z^2}\right)$$

$$\frac{\tau_{rz}(r,z)}{p_m} = -\frac{3}{2}\left(\frac{rz^2}{u^2+a^2 z^2}\right)\left(\frac{a^2 u^{1/2}}{a^2+u}\right)$$

where ν is Poisson's Ratio and u is

$$u = \frac{1}{2}\left[\left(r^2 + z^2 - a^2\right) + \sqrt{\left(r^2 + z^2 - a^2\right)^2 + 4a^2 z^2}\right].$$ (C.4)

Expressing these in terms of cylindrical coordinates is the most natural choice, due to the presence of an axis of rotational symmetry through the point of initial contact. The principal stresses then calculated at each point in the solid from σ_r, σ_θ, and σ_z by setting

$$\sigma_{1,3} = \frac{\sigma_r + \sigma_z}{2} \pm \sqrt{\left(\frac{(\sigma_r - \sigma_z)}{2}\right)^2 + \tau_{rz}^2}$$

$$\sigma_2 = \sigma_\theta.$$ (C.5)

These allow the derived quantities of local pressure and the maximum shear stress to be determined as functions of position;

$$\sigma_m(r,z) = \frac{\sigma_1 + \sigma_2 + \sigma_3}{3} = \frac{\sigma_r + \sigma_\theta + \sigma_z}{3}$$ (C.6)

$$\tau_{max}(r,z) = \frac{\sigma_1 - \sigma_3}{2} = \sqrt{\left(\frac{(\sigma_r - \sigma_z)}{2}\right)^2 + \tau_{rz}^2}.$$ (C.7)

Although these equations are not defined on the surface of the elastic medium, the values of the stress arbitrarily close to the surface may be determined from these equations by taking sufficiently small values of z [35].

APPENDIX D

CUMULATIVE FRACTION DISTRIBUTION

Assume an ensemble exists with n elements, and that the function $\dot{N}(t)$ describes the probability of an element of that ensemble entering the state p_1 per unit time. Further assume that the n elements initially exist in the state p_0, and that once an element enters the state p_1 that element remains in the state p_1. Consider finding the probabilistic distribution of elements displaying p_1 in time as a cumulative fraction F(t); that is, at each moment in time, return the relative fraction of the ensemble in state p_1. The rate of change of F(t) in time is

$$\frac{dF(t)}{dt} = (1 - F(t))\dot{N}(t) \tag{D.1}$$

since the rate of change of F(t) is directly proportional to the fraction of remaining elements in the state p_0, given by (1-F(t)), and to the probability of each one of those states entering the state p_1 per unit time, or $\dot{N}(t)$. This differential equation, when solved mathematically for F(t) as a function of time, gives

$$F(t) = 1 \pm \exp\left(-\int_0^t \dot{N}(t')dt'\right). \tag{D.2}$$

Since the fraction of the population in the state p_1 must be monotonically increasing, the only permissible form for the cumulative fraction function is then

$$F(t) = 1 - \exp\left(-\int_0^t \dot{N}(t')dt'\right). \tag{D.3}$$

APPENDIX E

GRAPHICAL REPRESENTATION OF RESULTS

The results of the nanoindentation experiments appear in graphical form in Figures E1, E2, and E3. Open circles represent the outcomes of single indentations. The curves defined by series of open circles are the experimentally determined cumulative fraction functions for the various sets of experimental conditions. The solid curves give the matching predicted cumulative fraction functions, as calculated by optimizing the dislocation nucleation function in Equation (3.3) for all available data. Equation (3.3) was chosen only to provide representative curves, and not as a result of any particular preference. Predictions generated by using other functions, with similar values of D when optimized for the available data, yielded predictions visually indistinguishable from the curves presented below.

For each of the figures, the horizontal axis represents the load applied to the surface of the sample during the relevant pop-in event. The vertical axis represents the fraction of indentations for a given set of conditions that exhibited pop-in before loading reached the appropriate value. Quantities that appear in the lower right corner of each graph indicate the conditions held constant for the indentations included in that figure. These may include sample orientation, system temperature, the time elapsed from the initiation of the loading function to reach maximum load, or the type of loading function. Function (a) or Function (b) specify the form of the loading function, as they appear in Figure 9.

Figure E1 includes each of the indentations used during this study. The cumulative fraction functions are organized to make the dependence of the statistics on loading rate visually explicit by holding all other system variables constant in a given figure, and allowing only the loading rate to vary. Figure E2 included selected experimental cumulative fraction functions from Figure E1. These are organized to make the dependence of the statistics on temperature explicit by holding all other variables constant in a given figure, and allowing only the temperature to vary. Other relationships between the loading conditions appear in graphical format in Figure E3.
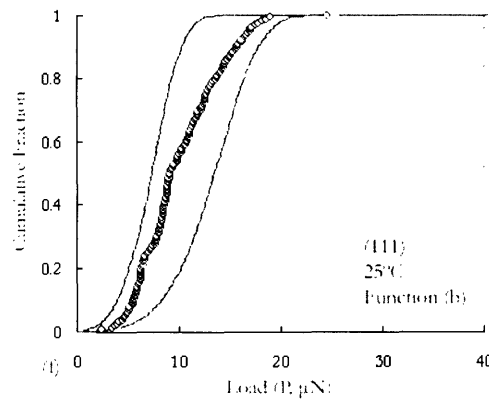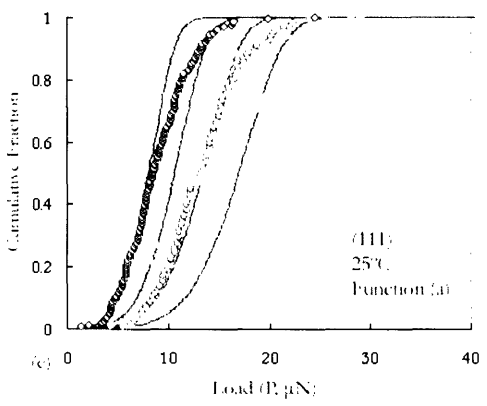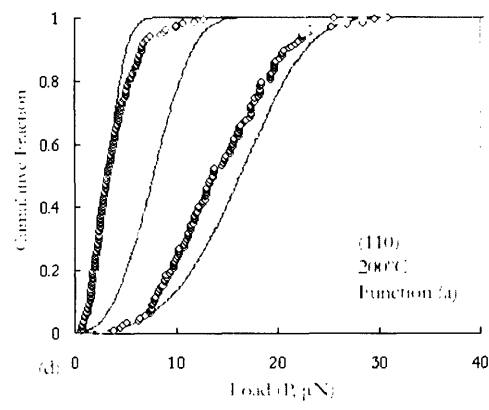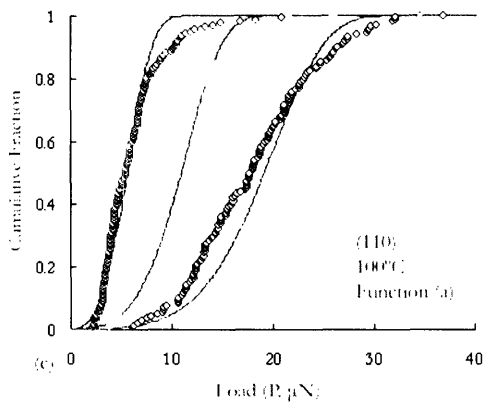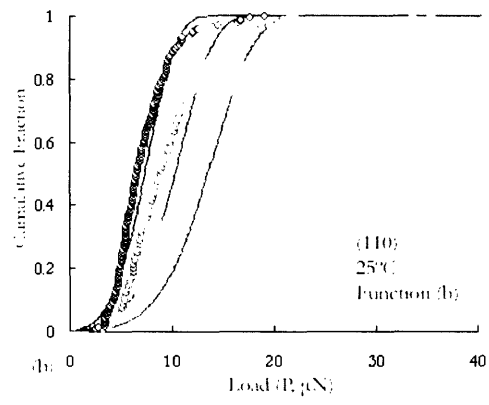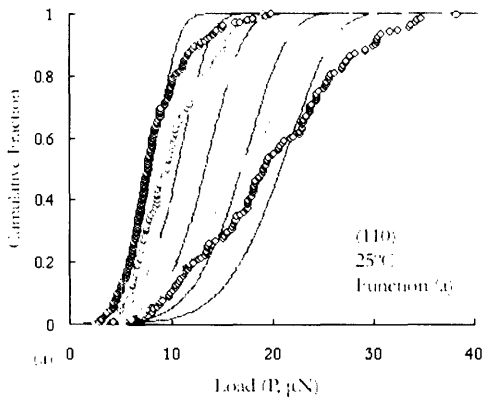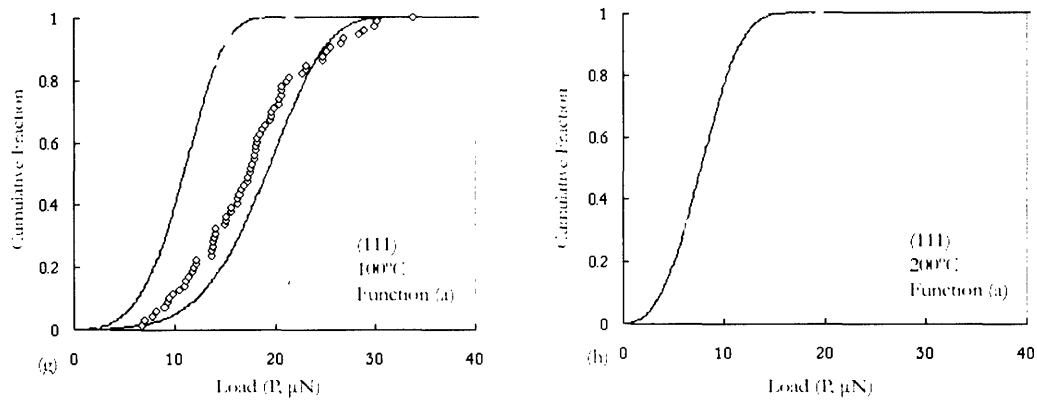
Figure E1: Graphical representation of all collected indentation data, presented to emphasize changes in statistical distribution with loading rate. Red, orange, yellow, green and blue experimental cumulative fraction curves represent indentations performed using 2, 0.6, 0.2, 0.06 and 0.02 seconds, respectively, to reach peak load. Notice that slower indentation rates lead to earlier pop-in. Predicted cumulative fraction functions appear as solid green lines. The relevant sample orientation, sample temperature, and loading function appear, in that order, in the lower right corner of each graph.
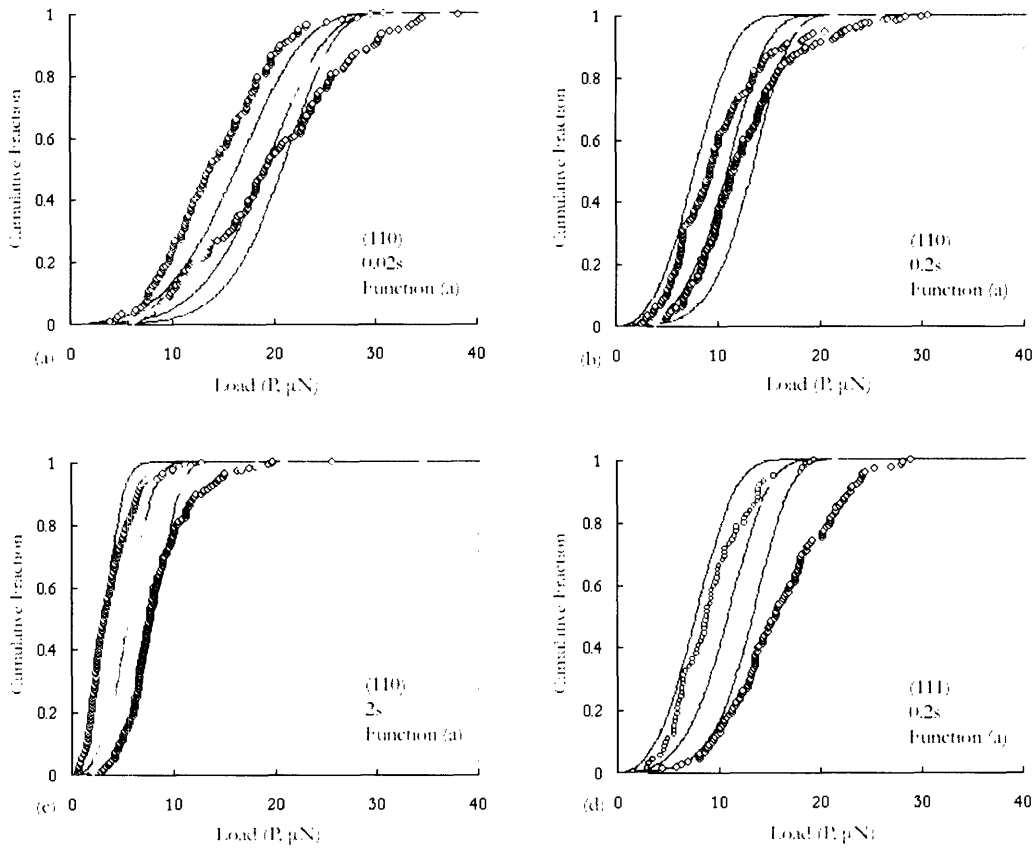
Figure E2: Graphical representation of selected indentation data from Figure E1, presented to emphasize changes in statistical distribution with temperature. Red, yellow, and blue experimental cumulative fraction curves represent indentations performed at temperatures of 200°C, 100°C, and 25°C, respectively. Notice that higher temperatures lead to earlier pop-in. Predicted cumulative fraction functions appear as solid green lines. The relevant sample orientation, time taken to reach peak load, and loading function appear, in that order, in the lower right corner of each graph.
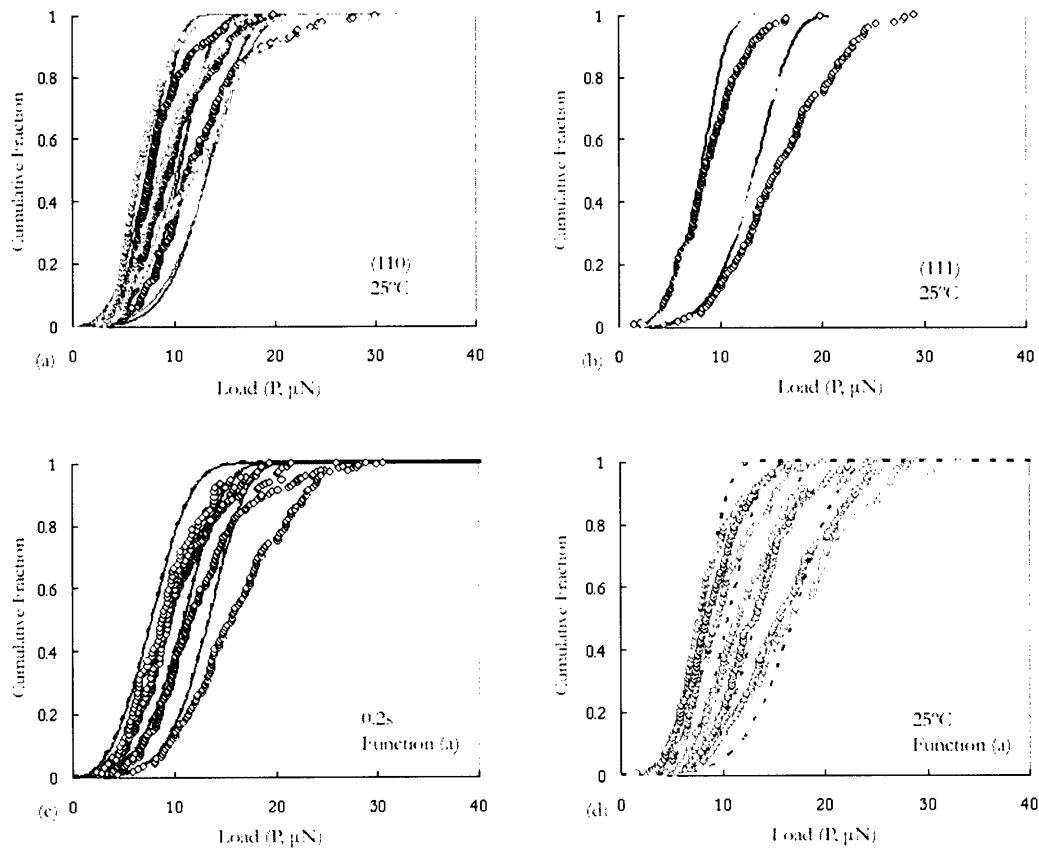
Figure E3: Graphical representation of selected indentation data from Figure E1, presented to emphasize relationships among variations in experimental conditions. (a) and (b) evaluate the statistics for different types of loading functions, while (c) and (d) examine the effects of sample orientation on the indentation statistics. Notice that compared to the temperature or loading rate dependence, the effects of variation in these conditions on the statistics is slight. Predicted cumulative fraction functions appear as solid or dashed lines. The conditions that remain constant for each graph appear in the lower right corner. (a) Effects of loading function on loading rate dependence for (110) sample. Function (a) appears in blue, Function (b) appears in green. Curves for 0.2s, 0.6s, and 2s to peak load depicted. (b) Effects of loading function on loading rate dependence for (111) sample. Function (a) appears in red, Function (b) appears in yellow. Curves for 0.2s and 2s to peak load depicted. (c) Effects of surface orientation on temperature dependence for 0.2s taken to peak load. (110) surface appears in blue, (111) surface appears in red. Curves for 200°C, 100°C, and 25°C depicted. (d) Effects of surface orientation on loading rate dependence for temperature of 25°C. (110) appears in yellow, (111) appears in green. Curves for 0.06s, 0.2s, 0.6s, and 2s depicted.

BIBLIOGRAPHY

1. Kittel, C., *Introduction to Solid State Physics*. 7 ed. 1996: John Wiley & Sons, Inc. 673.
2. Allen, S.M. and E.L. Thomas, *The Structure of Materials*. 1999, New York: John Wiley & Sons, Inc. 447.
3. Reed-Hill, R.E. and R. Abbaschian, *Physical Metallurgy Principles*. 3 ed. 1994, Boston: PWS Publishing Company. 926.
4. Cahn, R.W. and P. Haasen, eds. *Physical Metallurgy*. Vol. 2. 1996, North-Holland: New York.
5. Schuh, C. and A. Lund, *Application of nucleation theory to the rate dependence of incipient plasticity during nanoindentation*. Journal of Materials Research, 2004. **19**(7): p. 2152-2158.
6. Chiu, Y. and A. Ngan, *A TEM investigation on indentation plastic zones in Ni3Al(Cr,B) single crystals*. Acta Materialia, 2002. **50**(10): p. 2677-2691.
7. Kiely, J. and J. Houston, *Nanomechanical properties of Au (111), (001), and (110) surfaces*. Physical Review B, 1998. **57**(19): p. 12588-12594.
8. Tymiak, N., et al., *Acoustic emission monitoring of the earliest stages of contact-induced plasticity in sapphire*. Acta Materialia, 2004. **52**(3): p. 553-563.
9. Lorenz, D., et al., *Pop-in effect as homogeneous nucleation of dislocations during nanoindentation*. Physical Review B, 2003. **67**(17): p. -.
10. Asif, S. and J. Pethica, *Nanoindentation creep of single-crystal tungsten and gallium arsenide*. Philosophical Magazine A-Physics of Condensed Matter Structure Defects and Mechanical Properties, 1997. **76**(6): p. 1105-1118.
11. Corcoran, S., et al., *Anomalous plastic deformation at surfaces: Nanoindentation of gold single crystals*. Physical Review B, 1997. **55**(24): p. 16057-16060.
12. Bahr, D., D. Kramer, and W. Gerberich, *Non-linear deformation mechanisms during nanoindentation*. Acta Materialia, 1998. **46**(10): p. 3605-3617.
13. Gerberich, W., et al., *The Injection of Plasticity by Millinewton Contacts*. Acta Metallurgica et Materialia, 1995. **43**(4): p. 1569-1576.
14. Chiu, Y. and A. Ngan, *Time-dependent characteristics of incipient plasticity in nanoindentation of a Ni3Al single crystal*. Acta Materialia, 2002. **50**(6): p. 1599-1611.
15. Wang, W., C. Jiang, and K. Lu, *Deformation behavior of Ni3Al single crystals during nanoindentation*. Acta Materialia, 2003. **51**: p. 6169-6180.
16. Page, T., W. Oliver, and C. McHargue, *The deformation-behavior of ceramic crystals subjected to very low load (nano)indentations*. Journal of Materials Research, 1992. **7**(2): p. 450-473.
17. Bei, H., Z. Lu, and E. George, *Theoretical strength and the onset of plasticity in bulk metallic glasses investigated by nanoindentation with a spherical indenter*. Physical Review Letters, 2004. **93**(12): p. -.
18. Venkataraman, S., D. Kohlstedt, and W. Gerberich, *Continuous Microindentatin of Passivating Surfaces*. Journal of Materials Research, 1993. **8**(4): p. 685-688.
19. Thomas, R., et al., *The Mechanical Response of Gold Substrates Passivated by Self-Assembling Monolayer Films*. Science, 1993. **259**(5103): p. 1883-1885.
20. Michalske, T. and J. Houston, *Dislocation nucleation at nano-scale mechanical contacts*. Acta Materialia, 1998. **46**(2): p. 391-396.

21. Zuo, L., A. Ngan, and G. Zheng, *Size dependence of incipient dislocation plasticity in Ni3Al.* Physical Review Letters, 2005. **94**(9): p. -.

22. Kelchner, C., S. Plimpton, and J. Hamilton, *Dislocation nucleation and defect structure during surface indentation.* Physical Review B, 1998. **58**(17): p. 11085-11088.

23. Miller, R., L. Shilkrot, and W. Curtin, *A coupled atomistics and discrete dislocation plasticity simulation of nanoindentation into single crystal thin films.* Acta Materialia, 2004. **52**(2): p. 271-284.

24. Lilleodden, E., et al., *Atomistic simulations of elastic deformation and dislocation nucleation during nanoindentation.* Journal of the Mechanics and Physics of Solids, 2003. **51**(5): p. 901-920.

25. Pang, M., D. Bahr, and K. Lynn, *Effects of Zn addition and thermal annealing on yield phenomena of CdTe and Cd0.96Zn0.04Te single crystals by nanoindentation.* Applied Physics Letters, 2003. **82**(8): p. 1200-1202.

26. Gerberich, W., et al., *Indentation induced dislocation nucleation: The initial yield point.* Acta Materialia, 1996. **44**(9): p. 3585-3598.

27. Gerberich, W., et al., *An approach to dry friction and wear for small volumes.* Philosophical Magazine A-Physics of Condensed Matter Structure Defects and Mechanical Properties, 2002. **82**(17-18): p. 3349-3360.

28. Gouldstone, A., et al., *Discrete and continuous deformation during nanoindentation of thin films.* Acta Materialia, 2000. **48**(9): p. 2277-2295.

29. Suresh, S., T. Nieh, and B. Choi, *Nano-indentation of copper thin films on silicon substrates.* Scripta Materialia, 1999. **41**(9): p. 951-957.

30. Van Vliet, K., et al., *Quantifying the early stages of plasticity through nanoscale experiments and simulations.* Physical Review B, 2003. **67**(10): p. -.

31. Gannepalli, A. and S. Mallapragada, *Atomistic studies of defect nucleation during nanoindentation of Au(001).* Physical Review B, 2002. **66**(10): p. -.

32. Knap, J. and M. Ortiz, *Effect of indenter-radius size on Au(001) nanoindentation.* Physical Review Letters, 2003. **90**(22): p. -.

33. Bahr, D., D. Wilson, and D. Crowson, *Energy considerations regarding yield points during indentation.* Journal of Materials Research, 1999. **14**(6): p. 2269-2275.

34. Mann, A. and J. Pethica, *The effect of tip momentum on the contact stiffness and yielding during nanoindentation testing.* Philosophical Magazine A-Physics of Condensed Matter Structure Defects and Mechanical Properties, 1999. **79**(3): p. 577-592.

35. Fischer-Cripps, A.C., *Introduction to contact mechanics.* 2000, New York: Springer. xxi, 243 p.

36. Lund, A., A. Hodge, and C. Schuh, *Incipient plasticity during nanoindentation at elevated temperatures.* Applied Physics Letters, 2004. **85**(8): p. 1362-1364.

37. Pang, M. and D. Bahr, *Thin-film fracture during nanoindentation of a titanium oxide film-titanium system.* Journal of Materials Research, 2001. **16**(9): p. 2634-2643.

38. Kramer, D., K. Yoder, and W. Gerberich, *Surface constrained plasticity: oxide rupture and the yield point process.* Philosophical Magazine A-Physics of Condensed Matter Structure Defects and Mechanical Properties, 2001. **81**(8): p. 2033-2058.

39. Mann, A. and J. Pethica, *The role of atomic size asperities in the mechanical deformation of nanocontacts.* Applied Physics Letters, 1996. **69**(7): p. 907-909.

40. Pashley, M. and D. Tabor, *Adhesion and deformation properties of clean and characterized metal micro-contacts.* Vacuum, 1981. **31**(10-12): p. 619-623.

41. Pollock, H., *Contact adhesion between solids in vacuum: 2. Deformation and interfacial energy.* Journal of Physics D-Applied Physics, 1978. **11**(1): p. 39-54.

42. Velednitskaya, M., et al., *Investigation of the Deformation Mechanism of MgO Crystals Affected by Concentrated Load.* Physica Status Solidi, 1975. **32**: p. 123-132.

43. Rozhanskii, V. and M. Velednitskaya, *Electron Microscopy Investigation of the Surface Relief after Concentrated Load Deformation of NaCl Crystals.* Physica Status Solidi, 1971. **8**: p. 551-564.

44. Rodriguez de le Fuente, O., M. Gonzalez, and J. Rojo, *Dislocation configurations around a nanoindentation in the surface of a fcc metal.* Philosophical Magazine, 2003. **83**(4): p. 485-502.

45. Zielinski, W., et al., *Dislocation Distribution Under a Microindentation into an Iron-Silicon Single-Crystal.* Philosophical Magazine A-Physics of Condensed Matter Structure Defects and Mechanical Properties, 1995. **72**(5): p. 1221-1237.

46. Golovin, Y., A. Tyurin, and B. Farber, *Time-dependent characteristics of materials and micromechanisms of plastic deformation on a submicron scale by a new pulse indentation technique.* Philosophical Magazine A-Physics of Condensed Matter Structure Defects and Mechanical Properties, 2002. **82**(10): p. 1857-1864.

47. Farber, B., V. Orlov, and A. Heuer, *Energy dissipation during high temperature displacement-sensitive indentation in cubic zirconia single crystals.* Physica Status Solidi A-Applied Research, 1998. **166**(1): p. 115-126.

48. Farber, B., et al., *Mechanisms of energy dissipation during displacement-sensitive indentation in Ge single crystals at elevated temperatures.* Philosophical Magazine A-Physics of Condensed Matter Structure Defects and Mechanical Properties, 1998. **78**(3): p. 671-677.

49. Golovin, Y., A. Tyurin, and B. Farber, *Investigation of time-dependent characteristics of materials and micromechanisms of plastic deformation on a submicron scale by a new pulse indentation technique.* Journal of Materials Research, 2002. **37**(4): p. 895-904.

50. Fang, T., C. Weng, and J. Chang, *Molecular dynamics analysis of temperature effects on nanoindentation measurement.* Materials Science and Engineering A-Structural Materials Properties Microstructure and Processing, 2003. **357**(1-2): p. 7-12.

51. Walsh, P., et al., *Nanoindentation of silicon nitride: A multimillion-atom molecular dynamics study.* Applied Physics Letters, 2003. **82**(1): p. 118-120.

52. Yu, H., J. Adams, and L. Hector, *Molecular dynamics simulation of high-speed nanoindentation.* Modelling and Simulation in Materials Science and Engineering, 2002. **10**(3): p. 319-329.

53. Miller, R. and A. Acharya, *A stress-gradient based criterion for dislocation nucleation in crystals.* Journal of the Mechanics and Physics of Solids, 2004. **52**(7): p. 1507-1525.

54. Hirth, J.P. and J. Lothe, *Theory of dislocations.* 2nd ed. 1982, New York: Wiley. xii, 857.

55. Wo, P., L. Zuo, and A. Ngan, *Time-dependent incipient plasticity in Ni3Al as observed in nanoindentation.* Journal of Materials Research, 2005. **20**(2): p. 489-495.

56. Wo, P. and A. Ngan, *Incipient plasticity during nano-scratch in Ni3Al.* Philosophical Magazine, 2004. **84**(29): p. 3145-3157.

57. International, A., *ASM materials information, ASM handbooks online.* 2003, ASM International: Materials Park, OH.

58. Karato, S. and H. Jung, *Effects of pressure on high-temperature dislocation creep in olivine.* Philosophical Magazine, 2003. **83**(3): p. 401-414.

59. Shewmon, P.G., *Diffusion in solids.* 2nd ed. 1989, Warrendale, Pa.: Minerals, Metals & Materials Society. 246 p.

60. Seitz, F., *On the formation of dislocations from vacancies.* Physical Review, 1950. **79**: p. 890-891.

61. Johnson, K.L., *Contact mechanics.* 1985, Cambridge [Cambridgeshire]; New York: Cambridge University Press. xi, 452 p.